Chemical Engineering Journal 515 (2025) 163524

Contents lists available at ScienceDirect

Chemical Engineering Journal

journal homepage: www.elsevier.com/locate/cej

An innovative 'sorption-egg-hanced' reforming approach to producing highly pure green hydrogen from biomass-derived aqueous effluents

Javier Remón [a,*], Edurne Val-Planells [a], Avtar S. Matharu [b], Lucía García [a], Jesús Arauzo [a]

[a] Thermochemical Processes Group, Aragón Institute for Engineering Research (I3A), University of Zaragoza, C/Mariano Esquillor s/n, 50.018, Zaragoza, Spain
[b] Green Chemistry Centre of Excellence, University of York, Department of Chemistry, Heslington, York YO10 5DD, UK

ARTICLE INFO

Keywords:
Hydrogen production
Sorption-enhanced reforming
Eggshells
CaO-based sorbents
Hydrothermal treatments

ABSTRACT

The hydrothermal treatment of biomass forms large quantities of chemical-rich aqueous effluents. In the context of a zero-waste biorefinery, the latter represents a valuable resource for recovery and/or further functionalisation. This work reports for the first time the production of H_2 with in-situ CO_2 capture from the aqueous fraction of hydrothermally-processed almond hulls using a Ni-based catalyst coupled with a calcium-based sorbent derived from calcined eggshells. The effect of the reforming temperature and relative amounts of catalyst and sorbent (CaO) have been evaluated using a continuous reforming unit. The reaction temperature and the relative amount of catalyst directed the overall product distribution, with high temperatures favoured gas formation, and the catalyst allowed for lower temperatures to be used. Additionally, the temperature and the relative amount of sorbent significantly impacted the gas composition, with H_2 enrichment as the latter (calcined eggshells) increased. Process optimisation revealed that a gas with a highly high H_2 content (>95 vol%) can be obtained at 500 °C with relative amounts of catalyst and sorbent of 9 g catalyst min/g organics and 70 g CaO min/g organics, respectively. Such conditions allowed for capturing up to 90 % of the CO_2, which resulted in a very high H_2 production (0.12 g H_2/g organics, i.e., the stoichiometric value). This represents a step ahead for developing greener processes and opens the door to exploring novel avenues for process intensification, avoiding further downstream processes to ensure holistic, zero-waste biorefineries.

1. Introduction

The ongoing growth in the global population, connected with substantial increases in industrialisation and urbanisation, has resulted in the overconsumption of finite petroleum-based resources [1,2] and environmental pollution [3]. Such a paradigm needs urgent intervention by developing carbon-natural, sustainable and eco-friendly processes using renewable-based feedstocks to ensure a sustainable future for generations yet to come [4]. Lignocellulosic biomass is a renewable and carbon–neutral alternative to petroleum-based feedstocks for our future chemicals, materials and energy needs delivered through a biorefinery [5]. Where practical, biorefineries that utilise byproducts or underutilised lignocellulosic residues maximise the chemical resource potential whilst lowering the waste footprint [6,7]. Almond hulls, i.e., the external layer of the almond kernel and shell, are an interesting, underutilised, renewable feedstock, given that this part of the almond represents more than half of its total solid mass.[8] As the global demand for almonds continues to grow (from 0.7 Mt in 2007 to 1.5 Mt in 2020) [9], new valorisation strategies must be sought to manage almond leftovers [10].

Many thermochemical processes convert biomass into chemicals, material and bioenergy, such as pyrolysis, gasification and hydrothermal treatments [11]. Hydrothermal treatments (HTTs) include hydrothermal liquefaction and carbonisation, which use compressed hot water [12]. One of its significant returns is using a water-based medium, which dispenses with the requirement to dry the raw material. Therefore, this methodology is advantageous for high-moisture feedstocks, such as food waste. Furthermore, HTTs are milder compared to conventional pyrolytic and torrefaction processes and, thus, afford better product selectivity and properties [12–17]. Four main fractions or products are obtained through the HTT of biomass: gaseous, organic liquid (biocrude), solid (hydrochar), and an aqueous fraction. The gaseous fraction is a mixture of H_2, CO, CO_2 and CH_4, whose composition is determined by the processing parameters and the feedstock itself

* Corresponding author.
E-mail address: jrn@unizar.es (J. Remón).

https://doi.org/10.1016/j.cej.2025.163524
Received 22 November 2024; Received in revised form 10 March 2025; Accepted 6 May 2025
Available online 13 May 2025

and can be used as a gaseous biofuel (hydrogen or biogas) or as a precursor of liquid biofuels.[10,18] The aqueous fraction ranges between 40 and 60 % [19], containing a rich plethora of organic compounds: oligosaccharides, saccharides and oxygenated low molecular weight compounds [10,18]. This fraction is deemed waste and, thus, an economic and environmental burden [20,21]. Therefore, new valorisation strategies must be sought for this chemical-rich effluent and develop holistic zero-waste biorefineries within the confines of sustainability and circularity. However, these biorefinery water fractions are challenging to valorise as they comprise a complex pool of several oxygenated compounds in water.

Reforming processes using water in the gas and the liquid phase, i.e., steam reforming and aqueous phase reforming, are considered appropriate thermochemical routes to deal with these by-product water fractions as they simultaneously allow treating various organic compounds in water. Among these, catalytic steam reforming is a mature and widely used technology to valorise chemical-rich aqueous effluents. The process is conducted at relatively low temperatures (400–700 °C) under atmospheric pressure and converts organic matter within the effluent into a hydrogen-rich gas (up to ca. 70 vol%) [22,23]. Simultaneously, it decreases the feedstock organic content for safe discharge and the costly step of separating the water from the effluent is also avoided. This strategy aligns well with the current interest in developing new processes for producing sustainable carbon–neutral H_2 and connects with the emerging philosophy of using waste streams and by-products of biorefining processes. However, catalytic steam reforming of biomass-derived organic fractions produces carbon-containing gases in the effluent, primarily CO_2, CO and CH_4, and the desired H_2. Sorption-enhanced steam reforming (SESR) is a potential solution to enriching the H_2 content of the gaseous fraction. SESR uses a sorbent, commonly a metal oxide, to *in-situ* capture CO_2 produced by carbonation in the catalytic bed. This reduces its partial pressure and shifts the equilibrium of the water gas shift reaction ($CO + H_2O = CO_2 + H_2$) towards the production of H_2 [24–27]. This also leads to a decrease in the partial pressure of CO, which shifts the CH_4 reforming reaction ($CH_4 + H_2O = CO + 3H_2$) towards the production of H_2, increasing the relative amount of H_2 in the gas and, simultaneously decreasing the amounts of CO and CH_4 [24–27]. Besides, integrating H_2 production and purification in one unit intensifies the process, which also translates into eliminating downstream purification and separation stages. From an energetic perspective, the SESR process couples the endothermic H_2 production with the exothermic nature of the carbonation reaction. [28,29].

Selecting a suitable sorbent for *in-situ* CO_2 capture plays a pivotal role in SESR. The sorbent must be thermally stable, mechanically robust and durable at reforming temperatures. It must possess high and rapid CO_2 capture capacity as well as long-term cyclic stability. Economically, the sorbent needs to have low production costs and suitable regenerative (decarbonisation) capabilities [25,27]. SESR processes are currently designed in a mode where the reforming catalyst and the CO_2 sorbent are devised individually and subsequently mixed in the catalytic bed. Consequently, the natural subsequent step is the development of bifunctional materials that join catalytic and sorption capabilities simultaneously. However, producing active bifunctional materials is still challenging due to the possible irreversible interactions between the catalyst, adsorbent and support. Thus, present efforts in the early stage of this technology still focus on developing good catalyst-sorbent combinations. For example, the most used sorbents in SESR processes are split into three categories: i.) CaO-based sorbents, ii.) alkali-metal sorbents (Na_2ZrO_3, Li_2ZrO_3 and Li_4SiO_4) and iii.) hydrotalcite sorbents.

Calcium oxide is one of the most used sorbents because of its widespread availability, low cost, high CO_2 adsorption capabilities ((0.786 g CO_2/g CaO) and fast carbonation kinetics ((0.1–0.4 g CO_2/g CaO min) over steam reforming temperatures (400–700 °C) [25,27]. Several studies have highlighted that the temperature window for the carbonation reaction is between 500 and 600 °C [25,27], which makes catalytic steam reforming a suitable process to develop H_2 production with in-situ CO_2 capture. Besides, the carbonation reaction of CaO, leading to the formation of $CaCO_3$, is exothermic, which negates the overall endothermicity of the steam reforming process, increasing the energy efficiency of the whole process [25,27]. Regarding the availability of this material, there are mostly two different sources for CaO production, including natural and waste-derived Ca-containing materials and synthetic Ca sources [25,27]. The former group mostly comprises limestones and dolomites (consisting of calcium and calcium/magnesium carbonates), concrete, and natural conch-like materials/waste, such as crab shells, conch shells, carbide slags, steel slag, coal bottom ash and eggshells. These materials contain a high proportion of $CaCO_3$, which can be converted to CaO by calcination. Synthetic Ca sources include different reagents such as $Ca(NO_3)_2$, $Ca(CH_3COO)_2{\cdot}H_2O$, $C_{12}H_{24}O_{15}Ca$, $Ca(OH)_2$ and $CaCO_3$ [25,27].

Reprocessing agricultural waste and industrial by-products to produce CO_2 adsorbents helps decrease processing costs and remediate environmental pollution simultaneously. For example, egg shells, an unavoidable by-product from egg-processing industries, are a large-volume source of $CaCO_3$ (95 wt%), which can be converted into nanoporous CaO by calcination [30–33]. Egg manufacturing has increased substantially over the past few years, with around 87 million tons produced globally in 2020, and the vast majority of eggshells have been discarded as agricultural waste without any pre-treatment [25]. It is estimated that eggshell disposal in food processing incurs a food processing cost of over 1 million USD annually [34], which can be avoided by using them as a sorbent source. Given this, using eggshell-derived CaO in reforming processes needs to be explored to produce high pure (CO_2-free) H_2. The literature supports this hypothesis, as eggshell-derived CaO exhibits a greater CO_2 capture than commercial CaO due to the smaller particle size and higher exposed surface area for the carbonation reaction of the former than the latter [34,35]. Nevertheless, the literature on using CaO-derived eggshells as *in-situ* CO_2 adsorbents during H_2 production is limited. For example, Ayesha et al. reported that eggshell-derived CaO in the catalytic bed increased H_2 purity from 60 % to 77 % during methane reforming [34]. Li et al. used CaO derived from crab shells (rich in $CaCO_3$) as a sorbent during the sorption-enhanced gasification of pine sawdust to produce H_2 purities as high as 76 vol% [26]. Despite these publications highlighting the excellent capabilities of using eggshell-derived CaO to produce high-purity H_2 via thermochemical processes, to the best of the authors' knowledge, using this material for the SESR of biomass-derived organic effluents has not yet been reported.

Given this background and research opportunity, this publication reports for the first time the sorption-enhanced steam reforming of a residual aqueous effluent produced during the hydrothermal treatment of almond hulls to produce high-pure H_2. Our novel strategy uses CaO produced from eggshells as the sorbent, a new biorefining concept denoted as the 'sorption-egg-hanced reforming' approach, merged with a Ni-based catalyst with excellent reforming capabilities and deactivation resistance. Notably, the impact of the reforming temperature, mass of catalyst/organic mass flow rate, and mass of CaO/ organic mass flow rate on the process has been thoroughly investigated. The lack of publications reporting on using aqueous waste streams produced from the hydrothermal treatment of biomass, combined with the inherent renewable and novel approach exploring eggshells as alternative waste materials to produce Ca-based sorbents, demonstrates that our innovative 'egg-hanced' reforming strategy is a considerable step forward for the development of holistic and sustainable biorefineries to produce high-pure green H_2 from residual biomass-derived aqueous streams.

2. Experimental

Almond hulls were obtained from Marcona-type almonds harvested in Spain and were dried (60 °C for 24 h), chopped, sieved (100–200 μm) and stored in airtight containers. Their composition was characterised by fibre, proximate and ultimate analyses, with the results available in

our previous publications [10,36]. After each hydrothermal reaction, the products (biocrude, hydrochar, gas and aqueous fraction) were quantified and characterised, as reported elsewhere [36,37].

2.1. Hydrothermal treatment of almond hulls

The hydrothermal treatment of almond hulls was performed using a 500 mL, mechanically stirred, stainless steel autoclave reactor (Parr Instruments Company). Five experiments were conducted at previously optimised conditions, i.e., 300 °C, 160 bar, for 180 min, using a solid/water ratio of 25 wt% [10,36], to obtain the aqueous fraction for the subsequent sorption-enhanced steam reforming experiments. Following each hydrothermal treatment, the reactor was quenched with cold water to decrease its temperature to c.a. 35 °C. Then, a gas bag was used to collect a gaseous fraction, and its composition was determined using a Micro-Gas Chromatograph. Subsequently, the reactor was depressurised and opened to recover the liquid (biocrude and aqueous fraction) and solid (hydrochar) fractions, with the latter separated from the former by vacuum filtration. The biocrude was separated from the aqueous phase by liquid–liquid extraction and dried to remove the extraction solvents. Table 1 shows the formulae and analytical tools used to determine the gas, biocrude, aqueous fraction, and solid (hydrochar) yields, along with their key properties. Gas chromatography determined the gas composition, while elemental analysis and gas chromatography/mass spectrometry were used to address the physicochemical properties of the biocrude. The carbon-based chemical composition of the aqueous product was determined by high-performance liquid chromatography and elemental analysis, while elemental analysis characterised the hydrochar [10,39].

2.2. Preparation and characterisation of CaO from eggshells

Eggshells were obtained from Rua Restauración (University of Zaragoza, Rio Ebro Campus). Prior to calcination, the eggshells were washed with deionised water, dried (105 °C for 24 h), chopped, milled and sieved to a particle size between 200–315 μm. Then, they were calcined from 25 to 900 °C at a heating rate of 5 °C/min for 4 h and stored in airtight containers until further required. The original and calcined eggshells were analysed by Elemental Analysis (Leco TruSpec Macro analyser), X-ray diffraction (XRD), and Fourier Infrared Spectroscopy (FTIR). XRD spectra were collected at room temperature using a RIGAKU diffractometer, model Ru2500, provided with a rotating anode. The diffractometer operated at 40Kv and 80 mA and has a Cu anode and a graphite monochromator, which was used to select Kα radiation. The spectra were taken from (2Theta) 5 to 85°, with a step of 0.03° and a speed of 1 s/step. The "JCPDS-International Centre for Diffraction Data- 2000" database was used to identify the chemical species in the samples. FTIR analyses were conducted on a Bruker Vortex 70. The samples were mixed at 2 wt% with KBr and compressed with a 1200 kg/cm^2 torque for 1 min. The spectra were obtained in transmission mode using a MIR source and a DLaTGS detector, scanning from 400 to 4000 cm^{-1} with a resolution of 4 cm^{-1}.

2.3. Sorption-enhanced steam reforming: Catalyst and experimental rig

A co-precipitated Ni-Co/Al-Mg catalyst was prepared according to the literature [40]. This catalyst has 28 % Ni as Ni/(Ni + Co + Al + Mg) (atomic percentage), an atomic Mg/Al and Co/Ni ratios of 0.26 and 0.10, respectively, with a BET surface area of c.a. 132 m^2/g. It was chosen because of its good performance during the steam reforming of different organic effluents with similar chemical composition to the aqueous fraction used in this work, such as crude glycerol [41], bio-oil aqueous fractions [40,42,43] and cheese whey [23,44], and the sub- and supercritical water reforming of bio-oil [45].

The sorption-enhanced steam reforming experiments were conducted on a small bench-scale rig [40,42,43]. The set-up (Fig. 1) comprises a 25 cm height and 9 mm inner diameter stainless-steel fixed bed reactor placed inside an electric oven, with different feeding and collection/separation units. The feedstock was fed into the reactor with a HPLC pump, with N_2 being the carrier to serve as the internal standard for gas quantification, aid atomisation, and prevent the polymerisation of the aqueous fraction inside the feeding system as it is essential to ensure that the aqueous fraction enters the reactor in the liquid phase so that the vaporisation takes place in the upper part of the reactor prior to reaching the catalytic bed. The feed down-flow passed through the bed, which was composed of catalyst, sorbent (CaO from calcined eggshells), and inert sand. The temperature of the catalytic bed is monitored by a thermocouple located inside the reactor and in contact with the bed and controlled through a PID controller with variations lower than ± 1°C. The amount of inert sand was calculated to have the same bed length in all runs. The gaseous mixture exiting the reactor was passed through a condensation system, consisting of a steel vessel cooled using a Peltier

Table 1
Response variables and methods used during the Hydrothermal Treatment of Almond hulls.

Product	Response variable	Method/Equipment
Gas	$\text{Gas yield (\%)} = \frac{\text{mass of gas (g)}}{\text{mass of biomass (g)}} 100$	Micro-GC and reactor data
	$\text{Composition (vol. \%)} = \frac{\text{mol of each gas}}{\text{total mol of gas}} 100$	Micro-GC
	LHV (MJ/m^3 STP) = 0.1079 H_2 (vol.%) + 0.1263 CO (vol.%) + 0.3581 CH_4 (vol.%)	Estimated
Biocrude	$\text{Biocrude yield (\%)} = \frac{\text{biocrude (g)}}{\text{mass of biomass (g)}} 100$	Gravimetric
	$\text{C, H, O, N, (wt. \%)} = \frac{\text{mass of C, H, O, N (g)}}{\text{mass of biocrude (g)}} 100$	Elemental Analysis
	HHV (MJ/kg) = 0.3491C (wt.%) + 1.1783H (wt.%) – 0.1034O (wt.%) – 0.015 N (wt.%) + 0.1005 S (wt.%). [38]	Estimated
	$\text{Composition (Area \%)} = \frac{\textit{Area of each compound}}{\text{Total area of compounds}} 100$	GC/MS
Liquid (aqueous)	$\text{Liquid yield (\%)} = \frac{\text{liquid compounds (g)}}{\text{mass of biomass (g)}} 100 = 100 - (\text{Gas yield} + \text{Biocrude yield} + \text{Solid yield})$	Balance
	$\text{Composition (C – wt.\%)} = \frac{\sum \text{mass of C of each compound (g)}}{\text{total mass of C in solution (g)}} 100$	HPLC and Elemental Analysis
	$\text{C, H, O, N (wt. \%)} = \frac{\text{mass of C, H, O, N (g)}}{\text{mass of liquid (g)}} 100$	Elemental Analysis
Solid (hydrochar)	$\text{Solid yield (\%)} = \frac{\text{mass of solid (g)}}{\text{mass of biomass (g)}} 100$	Gravimetric
	HHV (MJ/kg) = 0.3491C (wt.%) + 1.1783H (wt.%) – 0.1034O (wt.%) – 0.015 N (wt.%) + 0.1005 S (wt.%). [38]	Estimated
	$\text{C, H, O, N (wt. \%)} = \frac{\text{mass of C, H, O, N (g)}}{\text{mass of solid (g)}} 100$	Elemental Analysis

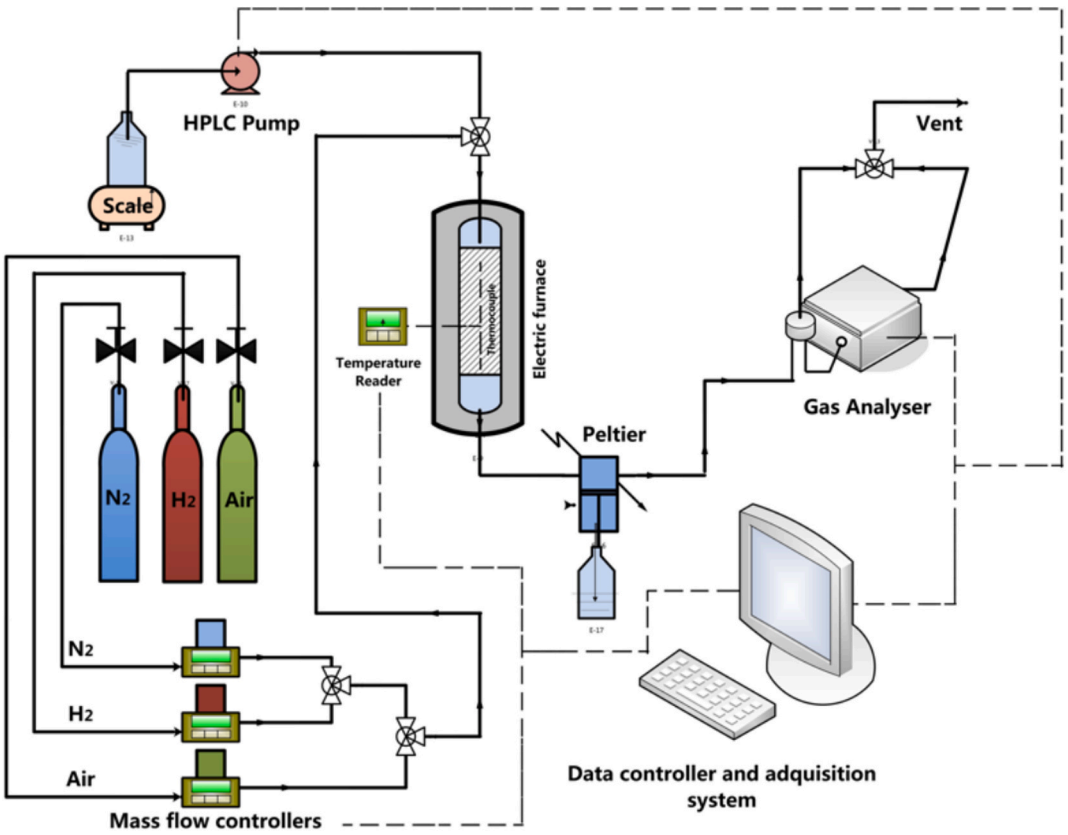

Fig. 1. Schematic of the SESR experimental system.

thermoelectric cell, to collect the condensable gases every 30 min to analyse the evolution of the liquid phase. The chemical composition of permanent gases leaving the condenser was determined online on a micro gas chromatograph.

After each experiment, a mass balance was conducted considering the feedstock fed in the reactor, the liquid phase collected, the gas produced and the solid recovered in the reactor. Mass balance closures higher than 98 % were attained for all the experiments. The catalytic bed was recovered at the end of each run, with the spent catalyst, spent sorbent, carbonaceous matter (char) and inert sand being recovered and fractionated. Firstly, carbonaceous matter and inert sand were recovered from the spent catalytic bed (catalyst and eggshells) by sieving due to the larger particle sizes of the former solids than those of the latter. Subsequently, the spent catalyst was separated from the eggshells by a magnet. The spent eggshells were subjected to elemental analysis to determine the carbon captured during the transformation of CaO to $CaCO_3$, with these data being then related to the adsorption capability of the solid. Besides, the C yields to solid at 30, 60, 90 and 120 min were used to calculate the overall C yield to solid obtained during the 2 h of reaction. This latter value was compared with the overall C yield to solid obtained experimentally (determined by elemental analysis after the reaction), and there were no statistically significant differences (p-value > 0.05) between both values.

Table 2 shows the response variables used to evaluate the influence of using eggshell-derived CaO as the sorbent during the sorption-enhanced steam reforming process. These include the overall reaction product distribution in a C basis, i.e., the C yields to gas, liquid and solid products (C gas %, C liq %, and C sol %), along with the detailed gas phase (N_2 and H_2O free, vol.% or mol.%) chemical composition. The total gas yield and the CO_2 capturing capability, expressed as the amount of C adsorbed with respect to the theoretical maximum C that could be adsorbed (C_{ad}/C_{max}), have also been calculated to study the adsorption capability of the eggshell-derived CaO. The thermodynamic

Table 2
Response variables and methods used during the SESR experiments of the aqueous fraction produced in the hydrothermal treatment.

Product	Response variable	Method
Gas	$\text{C yield to gas (\%)} = \frac{\text{mass of C in the gas (g)}}{\text{mass of C in the aqueous fraction (g)}} 100$	Micro GC
	$\text{Composition (vol. \%)} = \frac{\text{mol of gas}}{\text{total mol of gases}} 100$	Micro GC
	$\text{Yield (g/g org)} = \frac{\text{mass of gas}}{\text{mass of organics in the aqueous fraction}} 100$	
Liquid	$\text{C yield to liquid (\%)} = \frac{\text{mass of C in the liquid (g)}}{\text{mass of C in the aqueous fraction (g)}} 100$	Total Organic Carbon (TOC)
Solid	$\text{C yield to solid (\%)} = \frac{\text{mass of C in the solid (g)}}{\text{mass of C in the aqueous fraction (g)}} 100 = 100 - (\text{C yield to gas} + \text{C yield to liquid})$	Balance
	$CO_2 \text{ captured (C\%, m/m)} = \frac{\text{mass of C adsorbed (g)}}{\text{maximum mass of C as CaCO3 (g)}} 100$	Elemental Analysis

chemical composition (vol.%) of the gas phase and the thermodynamic yields to products (g of gas produced/ g of organics in the liquid effluent) were determined using the Gibbs Free Energy methodology. The data were obtained using the simulation software Aspen Hysys, employing a Gibbs Reactor and the Peng-Robinson fluid package for property calculations. In the simulation software, the dry molar feedstock elemental composition (C, H, O) was adjusted to different CO, CO_2, and H_2 amounts to define organic species. In detail, 100 g of aqueous fraction was simulated as 0.347 mol CO, 0.104 mol CO_2, 0.598 mol H_2 and 4.69 mol H_2O. This feedstock was introduced into the Gibbs Reactor along

with the N_2 used as the internal standard. The equilibrium chemical composition of the system was calculated by minimising the Gibbs Free Energy of a mixture composed of H_2, CO, CO_2, CH_4, C_2H_2, C_2H_4, C_2H_6, N_2 and H_2O at different temperatures. This allowed for calculating the thermodynamic volumetric chemical composition (N_2 and H_2O free) and gas yields at different temperatures. The thermodynamic results are listed in Table S.1 in the supporting information. The capture of CO_2 in the reactor modifies the equilibrium of the system as described above, shifting the water gas shift water gas shift reaction ($CO + H_2O = CO_2 + H_2$) [24–27] and the CH_4 reforming reaction ($CH_4 + H_2O = CO + 3H_2$) towards H_2 production.[24–27] This can lead to experimental yields of H_2 greater than those thermodynamically predicted without a sorbent. In such cases, the maximum H_2 yield is determined by the composition of the aqueous fraction (0.347 mol CO, 0.104 mol CO_2, 0.598 mol H_2 and 4.69 mol H_2O) considering the water gas shift reaction is completely shifted towards H_2 production, which results in maxima for the H_2 and CO_2 yields of 0.12 g H_2/g organics and 1.26 g CO_2/g organics, respectively.

2.4. Experimental Design, Response variables and Statistical analyses

The impact of the temperature (400–700 °C), the mass of catalyst/organic mass flow rate (W_{cat}/m_{org} = 4–16 g min/g) and the mass of calcinated eggshells/organic mass flow rate (CaO/m_{org} = 0–85 g min/g) were thoroughly addressed during the sorption enhanced catalytic steam reforming of the aqueous fraction obtained during the hydrothermal treatment of almond hulls. A 2-level, 3-factor Box-Wilson Central Composite Face Centred (CCF, α: ± 1) design was used to build the experimental design matrix. This methodology comprises 2^3 (8) experiments to cover linear effects and interactions, 4 centre points (repetitions at intermediate conditions) to determine error and variance, and 6 axial runs to resolve quadratic effects and interactions. An aqueous fraction liquid mass flow of 0.15 mL/min and a N_2 gas flow rate of 80 mL (STP)/min were used for all the experiments. Table 3 displays the processing conditions for the 18 runs conducted according to the experimental design.

The analysis of the results covers the effect of the processing parameters as well as their evolution with time. As for the latter, the results are first presented and split into four intervals of 30 min, with each interval providing the average value of the response variable obtained. These data (four per run, i.e., 0–30 min, 30–60 min, 60–90 min and 90–120 min) have been compared with a one-way ANOVA and the Fisher's least significant difference (LSD) test. The results obtained with these analyses are included graphically as LSD bars with 95 % confidence (p-value 0.05), which allows for direct comparison. Significant differences between any data pairs can be assured when their LSD bars do not overlap. Then, the effect of the operating variables on the process was studied, considering only the results corresponding to the first 30 min of the reaction, aiming at not including possible catalyst deactivation and sorbent saturation phenomena. These data were statistically analysed (ANOVA and Pareto test). The intervals of variations were codec to vary between −1 and + 1 to make them directly comparable. The ANOVA allowed for the selection of processing parameters and interactions, significantly impacting the results obtained during the first 30 min. The cause-effect Pareto test was used to classify these factors comparatively and their impact on the reforming results. Different interaction figures were built up with the ANOVA formulae created during the analysis of the 18 runs conducted. The effects of the processing conditions and interactions have been described graphically using interaction plots.

Table 3
Experimental conditions used in the SESR experiments of the aqueous fraction.

Run	Temperature (°C)	Mass of catalyst (g)	Mass of CaO (g)	Mass of sand (g)	W_{cat}/m_{org} (g min/g)	CaO/m_{org} (g min/g)
1	400	0.094	0	4	4	0
2	700	0.094	0	4	4	0
3	400	0.377	0	4	16	0
4	700	0.377	0	4	16	0
5	400	0.094	2	2	4	85
6	700	0.094	2	0	4	85
7	400	0.377	2	2	16	85
8	700	0.377	2	0	16	85
9	550	0.236	1	2	10	42.5
10	550	0.236	1	2	10	42.5
11	550	0.236	1	2	10	42.5
12	550	0.236	1	2	10	42.5
13	400	0.236	1	2	10	42.5
14	700	0.236	1	2	10	42.5
15	550	0.094	1	2	4	42.5
16	550	0.377	1	2	16	42.5
17	550	0.236	0	4	10	0
18	550	0.236	2	0	10	85

3. Results and discussion

3.1. Hydrothermal treatment of almond hulls

Almond hull hydrothermal treatment yielded four main products or fractions: gaseous, solid (hydrochar), biocrude, and aqueous. Table 4 lists the yields of these fractions and their most representative physicochemical properties. As for the aqueous fraction (product of interest in this research work), a yield of ca. 56 % was obtained, comprising c.a. 16 wt% of organics in water. The organic species primarily include sugar-derived compounds, mostly oligosaccharides, saccharides, and small amounts of carboxylic acids. The liquid phase does not contain other small oxygenates that can be produced with such a treatment as ketones, phenols or furans. These results align with the previous results obtained

Table 4
Product distribution and chemical properties of the products produced during the hydrothermal treatment of almond hulls at previously optimised conditions (300 °C, 160 bar, for 180 min and solid/water ratio of 25 wt% [10,36]).

Overall Product Distribution	
Gas yield (%)	4.81 ± 0.64
Solid yield (%)	25.28 ± 2.93
Biocrude yield (%)	14.41 ± 1.54
Aqueous fraction yield (%)	55.51 ± 2.12
Gas composition	
H_2 (vol.%)	1.69 ± 0.47
CO_2 (vol.%)	88.26 ± 2.75
CO (vol.%)	9.83 ± 0.53
CH_4 (vol.%)	0.22 ± 0.01
LHV (MJ/m^3 STP)	1.51 ± 0.32
Biocrude elemental analysis and HHV	
C (wt.%)	66.87 ± 2.44
H (wt.%)	6.26 ± 0.41
O (wt.%)	25.32 ± 2.91
N (wt.%)	1.55 ± 0.10
HHV (MJ/Kg)	28.08 ± 1.62
Hydrochar elemental analysis and HHV	
C (wt.%)	67.81 ± 0.58
H (wt.%)	4.99 ± 0.23
O (wt.%)	24.80 ± 0.89
N (wt.%)	2.421 ± 0.11
HHV (MJ/Kg)	26.95 ± 0.55
Aqueous fraction elemental analysis (raw basis)	
C (wt.%)	5.42 ± 0.26
H (wt.%)	10.56 ± 0.16
O (wt.%)	83.81 ± 0.22
N (wt.%)	0.21 ± 0.07
Aqueous fraction organic and water contents	
Organics (%, m/m)	15.71 ± 1.59
H_2O (%, m/m)	84.29 ± 1.59
Aqueous fraction chemical composition (wt.% C)	
Oligosaccharides	89.96
Saccharides	1.51
Carboxylic acids	9.11

during the hydrothermal treatment of this feedstock at the optimised conditions used in this work [10,36].

3.2. Production of CaO from eggshells

The eggshells used comprised 13.21 ± 0.12 % C and their subsequent calcination led to a mass loss of 53.97 ± 0.26 % with a change in colour from yellowish to white. These results are in close agreement based on the theoretical amount of C in $CaCO_3$ (12 wt%) and the mass loss associated with the transformation of $CaCO_3$ to CaO. The elemental analysis of the calcined eggshells revealed that the amount of C in the material was below the detection limit of the apparatus (<0.01 wt%), which further supports the transformation of $CaCO_3$ to CaO. Fig. 2 shows the X-ray diffraction (XRD) spectra of the original and calcinated eggshells. As for the former, the spectrum shows narrow, sharp peaks coinciding with $CaCO_3$ (calcite), with characteristic peaks at 2θ of 23, 29, 31, 36, 43, 48, 57, 65, 77 and 81 degrees, confirming the high $CaCO_3$ content in the eggshells. The calcined eggshells show narrow, sharp peaks at 2θ degrees of 32, 38 and 54, corresponding to CaO. Besides, broad peaks denoting the presence of $Ca(OH)_2$ primarily and, to a lesser extent, $Mg(OH)_2$, also appear in the spectrum due to the possible hydration of CaO. These results suggest a significant and almost complete transformation of $CaCO_3$ in eggshells to CaO during calcination, with a small amount of this latter solid being converted to $Ca(OH)_2$ during storage. Such a transformation agrees with the literature, showing that complete calcination occurs at temperatures higher than 800 °C [30,32,33].

Fig. 3 displays the FT-IR spectra of the eggshells and calcined eggshells. Eggshells show distinctive peaks at 1425, 876 and 711 cm^{-1}. These peaks account for carbonate vibrations. Notably, the first is linked to $CaCO_3$ in the eggshell matrix [30,32], while the other two result from in-plane and out-plane deformation modes, respectively [46]. The other peaks at 1796, 2514 and 3445 cm^{-1} are ascribed to the vibrations in the calcite structure of $CaCO_3$. Besides, bands linked to the O-H vibrations can be observed at 3445 and 1610 cm^{-1}, while organic matter (C-H str.) can be evidenced by the small bands in the region 3000–2800 cm^{-1}[30,32]. These comprise proteins in the outer membrane of eggshells (primarily collagen and glycoproteins). The calcined eggshells show significant peaks at 876, 1050, 1425 and 3642 cm^{-1}. The broad

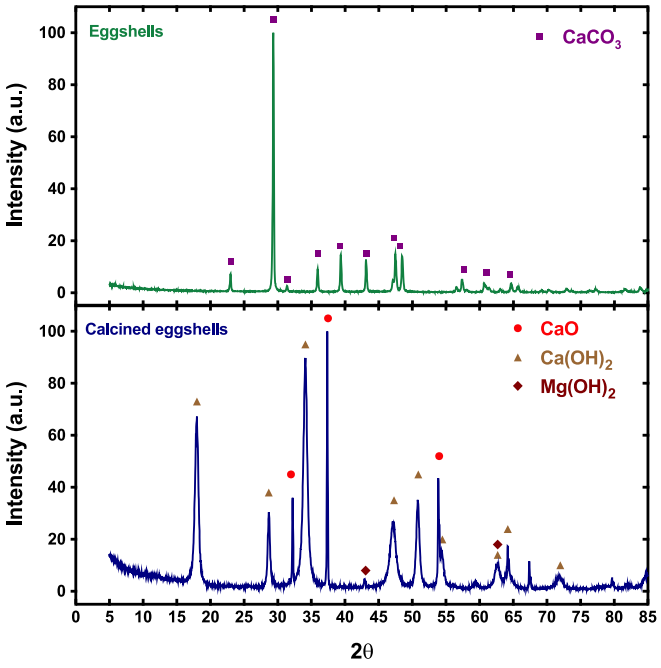

Fig. 2. XRD spectra of the eggshells and calcined eggshells.

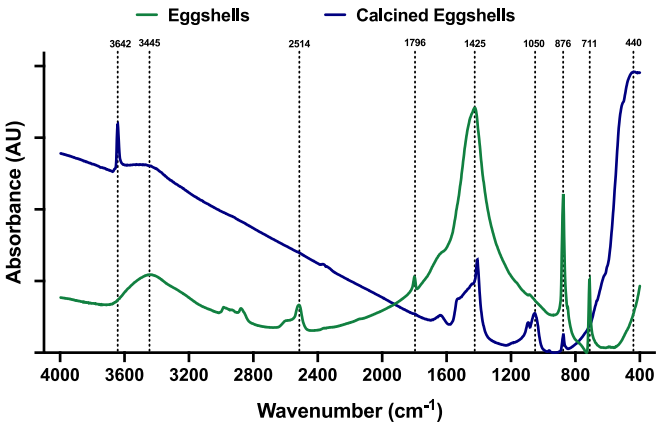

Fig. 3. FT-IR spectra of the eggshells and calcined eggshells.

peak at 3642 cm^{-1} corresponds to the O-H stretching vibration of (O–H) hydroxyl groups, which can be accounted for by the physical adsorption of water molecules on the core structure of CaO [47]. The peak at 876 cm^{-1} corresponds to vibrations of O–C-O typical of CaO, with those occurring at 440 cm^{-1} resulting from the stretching vibration frequency of Ca-O bonds [47,48]. The absorption peak at 1425 cm^{-1} results from CO_3^{2-} species [30,32], as described for eggshells, denoting that a small amount of $CaCO_3$ could not have been converted to CaO during calcination.

3.3. SESR of the aqueous fraction: Evolution over time

The SESR of the almond hull-derived aqueous fraction leads to the formation of a gas phase consisting of varying amounts of H_2, CO_2, CO and CH_4, a liquid effluent mainly comprising of un-reacted organic products in water, together with a solid residue made of carbonaceous residues (char and coke) and $CaCO_3$ formed during the reaction of CO_2 with the CaO in the calcined eggshells using as the sorbent. The evolutions over time of these fractions and those of the gas phase are described and discussed in sections 3.3.1 and 3.3.2, respectively. Table S.2 (supporting material) lists the detailed results of the SESR experiments.

3.3.1. Carbon yields to gas, liquid and solid

Fig. 4 shows the time evolution of the carbon yields to gas, liquid and solid products with respect to the initial carbon content of the effluent. These variations can be summarised into three groups. Runs 2, 4, 6 and 14 display the highest carbon yields to gas along with the lowest carbon yields to solid. These runs were conducted at a very high temperature (700 °C), favouring the complete vaporisation of the aqueous fraction (reducing carbonaceous solid due to incomplete vaporisation) and the reforming reactions of the vaporised organic molecules in the aqueous fraction. Different phenomena are noted depending on the relative amount of CaO (calcined eggshells) used. Runs 2 and 4 ($CaO/m_{org} = 0$ g min/g) display an initial increase in the C yield of gas and a drop in the C yield of solid between the first 30 min of the reaction. The aqueous fraction contains a high amount of oligosaccharides and saccharides (sugars), which are unstable at high temperatures and quickly decompose through pyrolysis, leading to the formation of char particles and gases during the vaporisation process, i.e., prior to reaching the catalytic bed [49]. As a result, part of the C content of the aqueous fraction is not effectively vaporised, primarily at low temperatures, leading to the formation of carbonaceous solid matter. This carbon content accumulates over the catalytic bed and can be progressively gasified with the excess water of the feed over the course of the reaction, leading to a decrease in the C yield to solid and an increase in the C yield to gas. Thus, the increases in the C yield to gas occurring along with decreases in the C yield to solid might account for the progressive gasification of

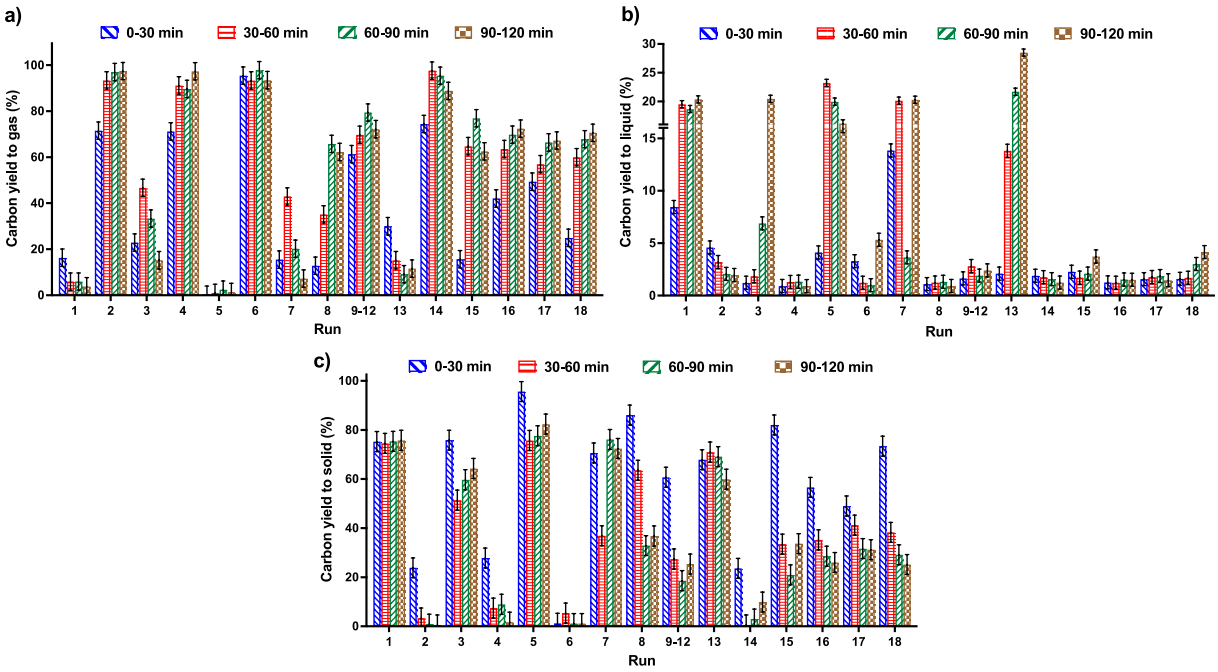

Fig. 4. Time evolution of the carbon yield to gas (a), carbon yield to liquid (b) and carbon yield to solid (c).

carbonaceous matter resulting from incomplete vaporisation of the organics in the aqueous fraction with the progress of the reaction. This phenomenon has been reported in other works dealing with the steam reforming of sugars [23,44]. Run 6, conducted with a high CaO/m_{org} ratio (85 g min/g), displays a high and steady C yield to gas and a meagre C yield to solid from the onset (0–30 min). Thus, CaO positively affects gasification [50], which decreases solid matter (char) production, boosting gas production. Run 14, conducted with an intermediate CaO/m_{org} ratio (42.5 g min/g), shows intermediate behaviour. The C yield to gas increases at the beginning and then decreases. This variation is opposite in the C yield to solid, i.e., an initial decrease and a subsequent increment. The lower CaO/m_{org} ratio (42.5 vs 85 g min/g) hinders the positive CaO effect on char gasification. The increase in solid matter over time is due to the gradual formation of char. Furthermore, the progressive accumulation of solid matter (char) in the upper part of the reactor hampers the effective atomisation and vaporisation of the aqueous fraction, as liquid vaporisation is not as effective when the liquid drops interact with solid particles during vaporisation, resulting in bigger droplet sizes. Thus, evaporation occurs at lower heating rates, which boosts char formation over time [51]. Such a phenomenon decreases the reaction rate of the gasification reactions of the carbonaceous deposits and increases the C yield to solid at the expense of the C yield to gas. Similar trends have been reported during steam reforming of several saccharides (glucose, xylose and sucrose) [49,52].

Runs 3, 7, 9–12, 14 and 15 initially show low and high C yields to gas and solid, respectively, with increases in the former and decreases in the latter during the first 60 min of the reaction. At 120 min, the C yield to gas decreases at the expense of the C yield to solid. Runs 3 and 7 were conducted at 400 °C, which promoted carbonaceous solid formation due to incomplete feed vaporisation. As these runs were conducted with a high catalyst amount (W_{cat}/m_{org} = 16 g min/g), the initial drop in the C yield to solid and the increment in the C yield to gas could be the result of the gasification and subsequent reforming of these solid residues. However, as the reaction proceeds, the reaction rate of solid production might be faster than that of their gasification, which can explain the variations over time for the C yields to gas and solid. Additionally, char accumulation in the upper part of the reactor hampers the atomisation and vaporisation of the aqueous fraction, as described above [51]. Runs 9–12, 14 and 15 were conducted using temperatures between 550 and 700 °C with different W_{cat}/m_{org} and CaO/m_{org} ratios. Such experiments display initial increments and drops in the C yields to gas and solid, respectively. After that, opposite variations are observed with respect to time, which may be due to the formation of carbonaceous matter and, additionally, from the CO_2 captured in the form of $CaCO_3$ (increasing solid formation) and its saturation over time of the sorbent (CaO from calcined eggshells) in a multi-step process [25,27]. The third group includes Runs 1, 5 and 13, conducted at a low temperature (400 °C), which results in high C yields to solid and low C yields to gas. This seems to indicate that such a temperature is not high enough to vaporise the feed effectively, leading to the formation of solid residues.

As for the evolution of the C yield to liquid over time, there are two distinctive trends: i.) Runs 1, 3, 5, 7 and 13 show relatively high C yields to liquid with progressive increments with the development of the reaction. Such runs were done at a low temperature (400 °C), where the reforming reaction is not favoured [23,44]. Besides, the possible deactivation of the catalyst over time might explain the progressive increment of the C yield to liquid, which takes place along with a drop in the C yield to gas; and, ii.) the C yield to liquid for the remaining runs, conducted at temperatures between 550 and 700 °C, is meagre (lower than 5 %), as liquid production is not thermodynamically promoted at such temperatures [25]. As a result, the effectively vaporised feed is converted to gaseous products, with the rest evolving towards solid residues.

3.3.2. *Gas phase volumetric composition*

The gas phase (Fig. 5) primarily involves a mixture of H_2 (43–98 vol %) and CO_2 (1–58 vol%), with small amounts of CO (0–11 vol%) and CH_4 (0–17 vol%). The relative amounts of these compounds alter over time, with H_2 and CO_2 showing the most significant variations as the major components in the gas mixture. The variations occurring for the concentrations of CO and CH_4 are not significant from a practical point of view.

Two distinctive behaviours are observed in the time evolution of H_2 and CO_2. On the one hand, diminishments over time for the proportions of H_2 and increases in the relative amounts of CO_2 occur for Runs 1, 5, 7, 9–12, 13–16 and 18. These variations are substantially more marked during the first hour of reaction and can have two distinctive origins. The variations observed for Runs 1, 5, 7 and 13 are assumed to be related

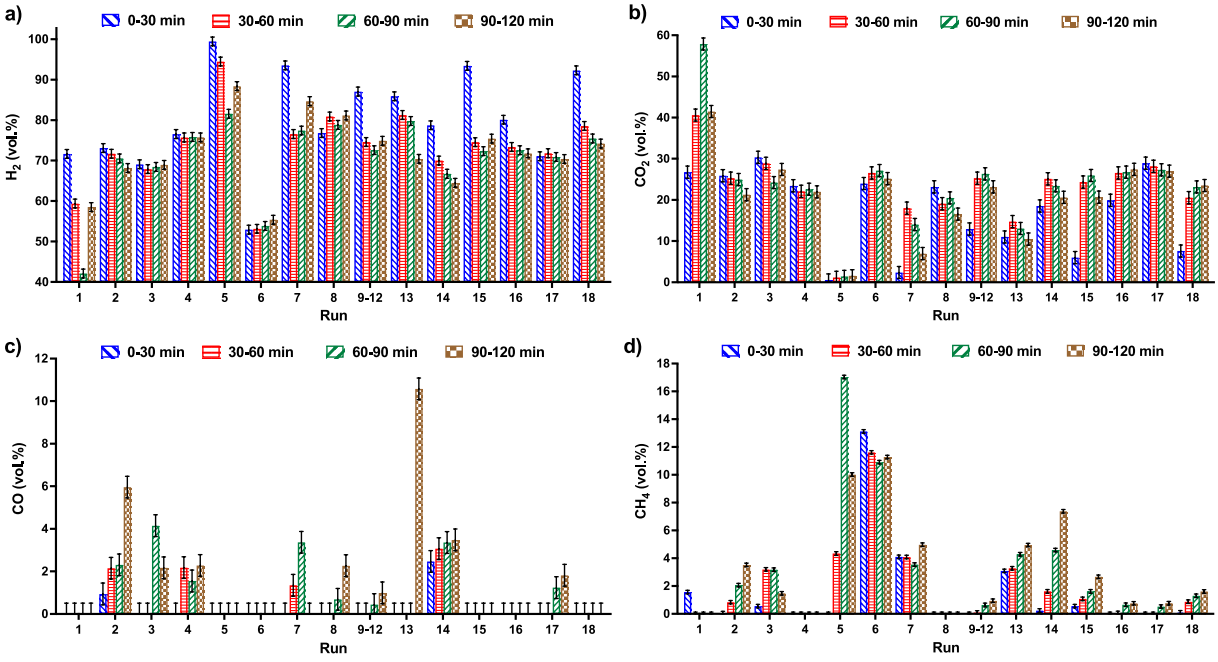

Fig. 5. Time evolution of the relative amounts of H_2 (a), CO_2 (b), CO (c) and CH_4 (d) in the gas phase.

to the formation and gasification of carbonaceous matter resulting from ineffective and incomplete feed vaporisation at a low (400 °C) temperature [23,44]. Thus, most of the C is in the solid product, producing a gas with a high H_2 content. Over time, the subsequent gasification of this carbonaceous matter enriches the amount of C in the gas, which increases the relative amount of CO_2 and drops the proportion of H_2. On the other hand, Runs 9–12, 14, 15, 16 and 18 were conducted at higher temperatures (550–700 °C) at which gas formation via vaporisation and/or reforming is promoted [23,44]. For these latter experiments, the high H_2 concentration in the gas is due to the CO_2-adsorption propensity of calcined eggshells (CaO) in the catalytic bed. With the development of the reaction, the adsorption capacity of CaO decreases due to saturation, increasing the concentration of CO_2 at the expense of the relative amount of H_2 [25,27].

3.4. SESR of the aqueous fraction: Processing conditions influence

The full impact of the reforming temperature, mass of catalyst/ organic mass flow rate (W_{cat}/m_{org}) and mass of CaO/ organic mass flow rate (CaO/m_{org}) over the first 30 min on the overall product distribution (C yields to gas, liquid and solid) and the gas phase volumetric composition is detailed in Table 5.

3.4.1. Carbon yields to gas, liquid and solid

The C yields to gas, liquid and solid vary by 0–95 %, 1–14 % and 1–96 % during the first 30 min of reaction. The cause-effect Pareto test shows that the temperature impacts the C yields to gas and solid, followed by the W_{cat}/m_{org} and CaO/m_{org} ratios (including linear and quadratic impacts). Besides, there are significant interactions between temperature and W_{cat}/m_{org} that have a substantial impact on these yields. Likewise, the coefficients of the terms in the ANOVA models for the C yields to gas and solid are very similar but with an opposite sign, indicating that increases in the C yield to gas leads to decreases in the C yield to solid and *vice versa*. The temperature and some interactions between this variable and the W_{cat}/m_{org} ratio are the parameters exerting the most influential impact on the C yield to liquid. Fig. 6 plots

Table 5
Relative impact of the processing parameters on the overall carbon yields and detailed composition of the gas phase during the first 30 min of reaction.

	R^2	Ind.	A	B	C	AB	AC	BC	A^2	B^2	C^2	ABC	A^2B	A^2C	AB^2
C yield to gas (%)	0.99	38.15	24.06 (29)	13.2 (4)	−8.24 (10)	−13.11 (14)	n.s. n.s.	−9.21 (10)	12 (5)	−11.36 (7)	n.s. n.s.	−11.38 (12)	−20.83 (10)	n.s. n.s.	n.s. n.s.
C yield to liquid (%)	0.99	1.73	n.s. n.s.	−0.435 (4)	12.2 (9)	−1.04 (9)	−1.18 (10)	2.31 (19)	n.s. n.s.	n.s. n.s.	n.s. n.s.	−1.93 (16)	n.s. n.s.	0.8963 (8)	−2.22 (24)
C yield to solid (%)	0.99	60.56	−22.27 (25)	−6.66 (4)	10.61 (9)	14.15 (14)	2.56 (3)	6.9 (7)	−13.69 (6)	9.89 (6)	n.s. n.s.	13.3 (13)	20.74 (9)	−5.85 (3)	n.s. n.s.
H_2 (vol.%)	0.99	87.02	−3.58 (14)	−6.66 (1)	10.61 (12)	4.48 (9)	−9.01 (18)	2.13 (4)	−4.86 (12)	n.s. n.s.	−5.47 (7)	2.97 (6)	9.02 (8)	−6.57 (6)	−3.2 (3)
CO_2 (vol.%)	0.99	13.01	4.4 (14)	6.94 (5)	−10.66 (26)	−1.08 (3)	6.5 (19)	n.s. n.s.	1.57 (10)	n.s. n.s.	5.04 (9)	n.s. n.s.	−6.68 (9)	3.62 (5)	n.s. n.s.
CO (vol.%)	1	0	1.24 (21)	n.s. n.s.	n.s. n.s.	−0.12 (6)	−0.12 (6)	0.12 (6)	1.23 (14)	n.s. n.s.	n.s. n.s.	0.12 (6)	−0.12 (6)	−0.12 (6)	−1.12 (27)
CH_4 (vol.%)	1	0	−1.43 (3)	−0.28 (8)	−0.28 (8)	−2.03 (14)	1.39 (10)	−0.9938 (7)	1.67 (11)	0.28 (2)	0.055 (1)	−2.27 (16)	−0.9812 (3)	1.82 (6)	2.3 (7)

A = Temperature, B = W_{cat}/m_{org}, C = CaO/m_{org}, n.s. = not significant with 95 % confidence.
Response = Ind. + Coefficient A·A + Coefficient B·B + Coefficient C·C + Coefficient AB·A·B + Coefficient AB·A·B + Coefficient BC·B·C + Coefficient A^2·A^2 + Coefficient B^2·B^2 + Coefficient C^2·C^2 + Coefficient ABC·A·B·C + Coefficient A^2B·A^2·B + Coefficient A^2B·A^2·B + Coefficient AB^2·A·B^2 + Coefficient A^2B^2·A^2·B^2.
Standardised codec formula: all operating variables vary between −1 and + 1. Numbers in brackets show the relative influence (%) of each factor on the response variable.

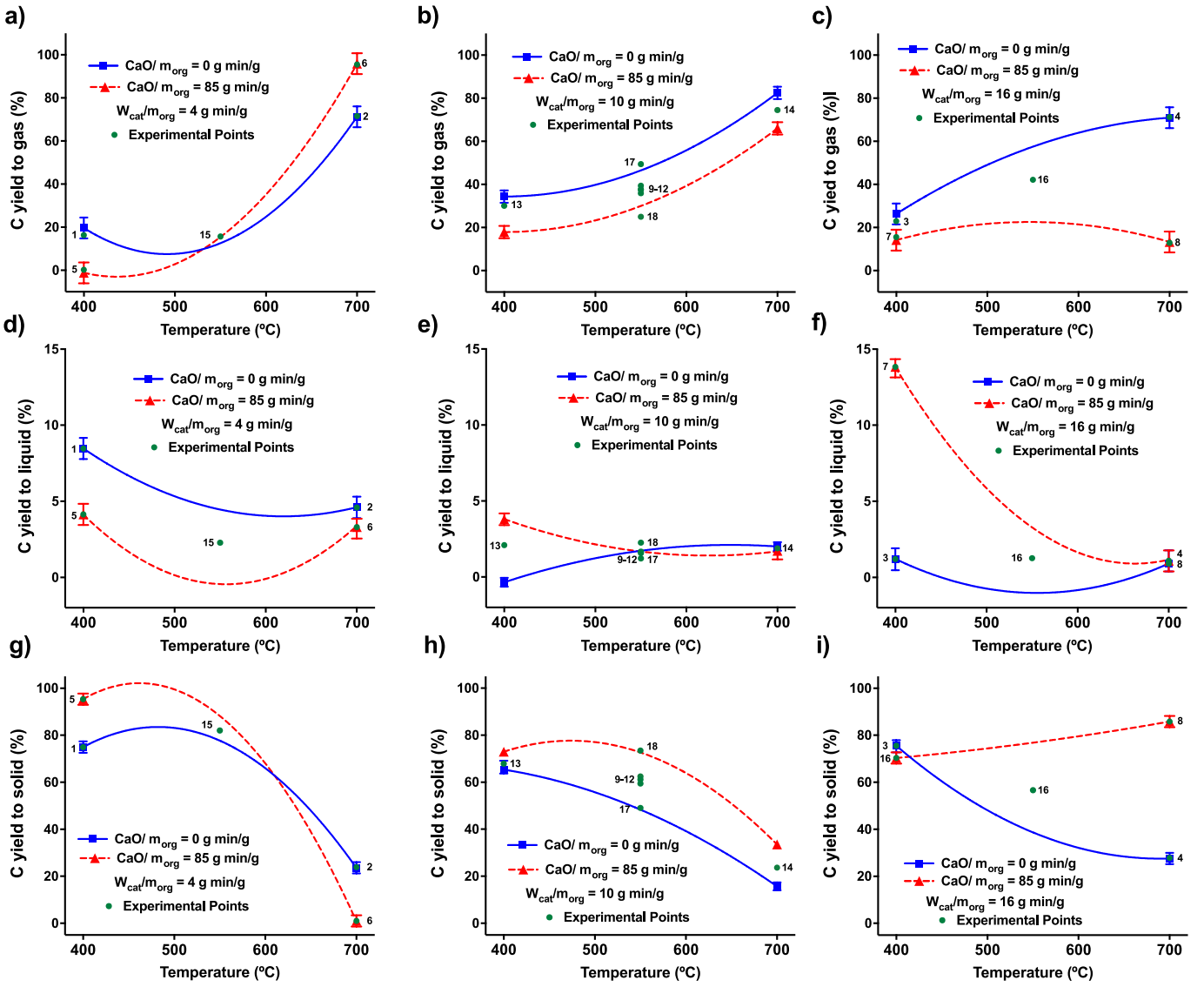

Fig. 6. Processing parameters (temperature, W_{cat}/m_{org} and CaO/m_{org} ratios) impact on the C yields to gas (a, b, c), liquid (d, e, f) and solid (g, h, i).

the influences on the reaction temperature and W_{cat}/m_{org} and CaO/m_{org} ratios on the product distribution on a C basis. Fig. 6 a, d and g show the influence of the temperature on the C yields to gas, liquid and solid as a function of the amount of CaO (CaO/m_{org} = 0 and 85 g min/g), with a W_{cat}/m_{org} ratio of 4 g min/g. Additionally, Fig. 5 b/e/h and c/f/i plot these influences for a W_{cat}/m_{org} ratio of 10 and 16 g min/g, respectively.

As for the C yields to gas and solid, Fig. 6 shows that regardless of the processing conditions, increases in the C yield to gas lead to decreases in the C yield to solid and *vice versa*. In general, these variations are accounted for by increases in the temperature. The temperature positively influences the process, increasing its kinetics and promoting its thermodynamics due to the endothermic character of the reforming reactions [24–27]. Also, increasing the temperature facilitates the complete vaporisation of the feed, ensuring its transformation to gas and diminishing the formation of carbonaceous solid residues [49,52]. Despite these general statements, the variations observed with the temperature in the C yields to gas and liquid are dependent on the relative amount of sorbent and catalyst used (CaO/m_{org} and W_{cat}/m_{org} ratios). When the process is conducted without a sorbent (CaO/m_{org} = 0 g min/g), the impact of the temperature depends on the amount of catalyst. With a low amount of catalyst (W_{cat}/m_{org} = 4 g min/g), the C yield to gas is low between 400 and 550 °C due to the high C yield to solid (Fig. 6 a/g). A subsequent temperature rise to 700 °C upsurges the C yield to gas at the expense of the C yield to solid due to the positive temperature impact on the process [49,52]. Increasing the W_{cat}/m_{org} ratio from 4 to 10 g min/g raises the C yield to gas and drops the C yield to solid (Fig. 6 a/g vs b/h vs c/i). Two different temperature-related phenomena account for these variations: i.) at low temperatures, increasing the relative amount of catalyst promotes carbonaceous residue gasification [23,44]; and ii.) at high temperatures, gas formation is promoted due to a more efficient vaporisation of the feedstock. Under such conditions, loading a greater amount of catalyst facilitates the reforming reactions and decreases the temperature to achieve maxima for the C yield to gas and minima for the C yield to solid (c.a. 700 °C for W_{cat}/m_{org} = 10 g min/g and c.a. 600 °C for 16 g min/g). As a result, steady evolutions are attained for the C yield to gas and solid between 600 and 700 °C with the highest amount of catalyst (W_{cat}/m_{org} = 16 g min/g), which promotes the process energy as lower temperatures are required.

An increase in sorbent (CaO/m_{org} ratio) alters the impacts of the temperature and catalyst amount. When the process is conducted with the highest amount of sorbent (CaO/m_{org} = 85 g min/g), the influence of the temperature varies depending on the relative amount of catalyst. For W_{cat}/m_{org} ratios between 4 and 10 g min/g (Fig. 6 a/g and b/h), the

impact of the temperature is similar to that described in the absence of a sorbent, i.e., a temperature increment upsurges the C yield to gas at the expense of the C yield to solid. Conversely, the temperature does not significantly influence the C yields to gas and solid when a high proportion of catalyst (W_{cat}/m_{org} = 16 g min/g) is used. Two complementary phenomena account for these variations: i.) gas formation is not promoted at low temperatures, with the organics in the feedstock evolving towards solid residues [23,44], and ii.) the presence of CaO in the catalytic bed increases solid production as the formed CO_2 is transformed into $CaCO_3$, decreasing the C yield to gas and increasing the C yield to solid. As a result, solid formation at low temperatures accounts for the formation of carbonaceous matter from incomplete vaporisation

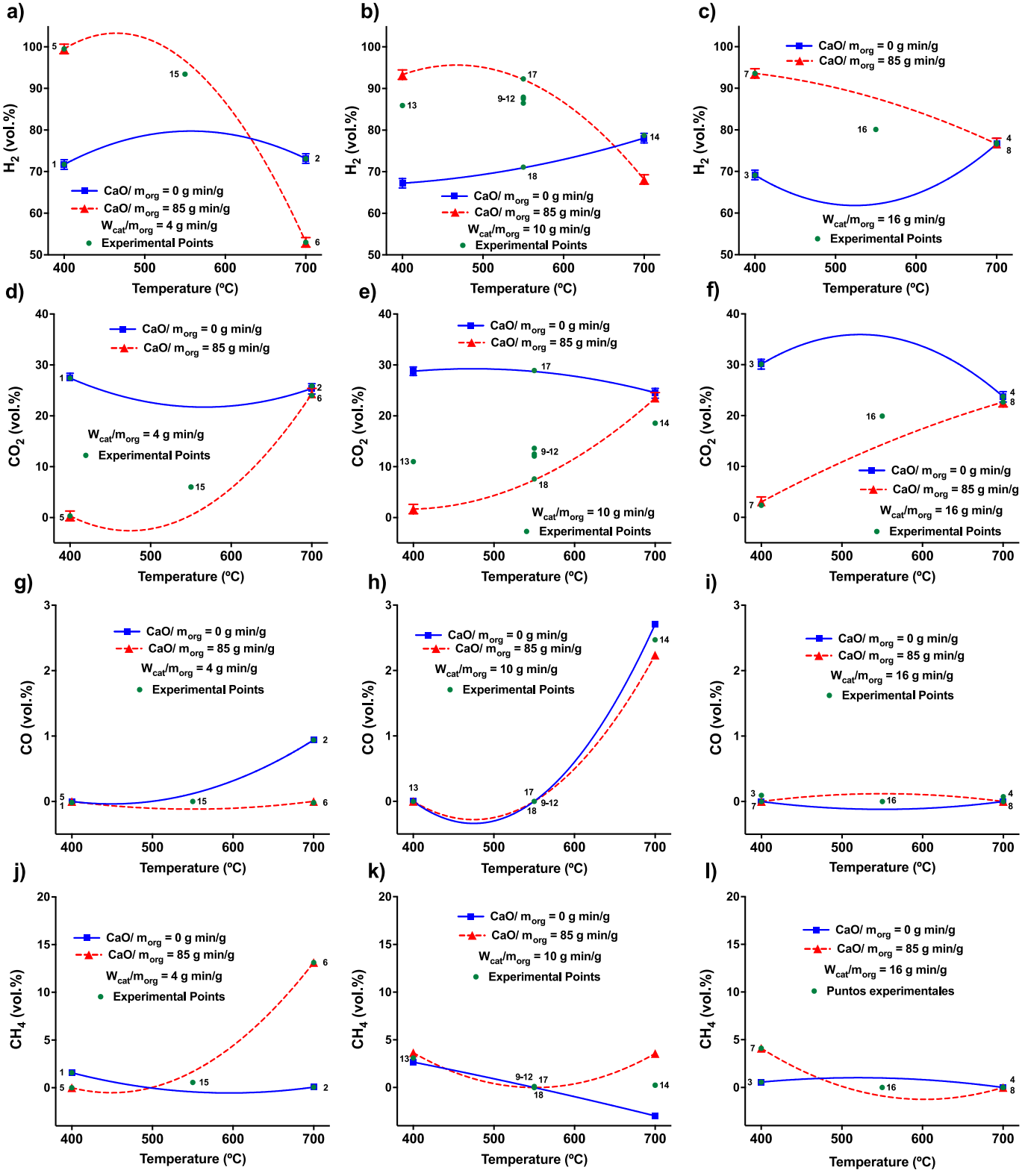

Fig. 7. Processing parameters (temperature, W_{cat}/m_{org} and CaO/m_{org} ratios) impact on the volumetric composition of the gas phase.

along with $CaCO_3$ from carbonation [25,27]. Likewise, the impact of the relative amount of catalyst when the process is conducted with the highest amount of sorbent (CaO/m_{org} = 85 g min/g) depends on the temperature. Between 400 and 550 °C, increasing the W_{cat}/m_{org} from 4 to 16 g min/g (Fig. 6 a/g vs b/h vs c/i) promotes gas formation. This accounts for the beneficial catalyst impact on the gasification of the carbonaceous matter [23,44], dropping the C yield to solid at the expense of the C yield to gas. Contrariwise, such an increment in the W_{cat}/m_{org} ratio drops the C yield to gas and upsurges the C yield to solid between 550 and 700 °C due to the catalyst positive impact on the process [23,44], promoting the reforming reaction leading to H_2 and CO_2. An increase in the amount of CO_2 in the presence of the maximum amount of CaO promotes $CaCO_3$ formation, which consequently drops the C yield to gas and upsurges the C yield to solid.

As a result of these variations, the impact of the relative amount of sorbent depends on the relative amount of catalyst. For a low amount of catalyst (W_{cat}/m_{org} from 4 g min/g), the impact of the CaO/m_{org} ratio depends on the temperature. Between 400 and 550 °C, increasing the CaO/m_{org} ratio leads to increases in the C yield to solid at the expense of the C yield to gas. Such variations result from forming carbonaceous matter by incomplete vaporisation and $CaCO_3$ by carbonation. From 550 to 700 °C, such an increment in the CaO/m_{org} ratio raises the C yield to gas and diminishes the C yield to solid. These variations indicate that CaO exerts a catalytic impact on the reforming process, leading to CH_4 formation. This development is in line with the literature [50], and it is more noticeable using low W_{cat}/m_{org} ratios (Fig. 7 j), as a higher amount of catalyst can mask the catalytic features of CaO in the process. For a higher proportion of catalyst (W_{cat}/m_{org} ratios from 10 to 16 g min/g), an increase in the relative amount of CaO from 0 to 85 g min/g leads to diminishments in the C yield to gas and increments in the C yield to solid, regardless of the temperature. Under these conditions, reforming reactions are promoted, leading to CO_2 formation. As a result, upsurging the amount of CaO in the catalytic bed promotes $CaCO_3$ formation, capturing CO_2 from the gaseous stream, which results in simultaneous rises and diminishments in the C yield to solid and gas, respectively.

The impact of the processing conditions on the C yield to liquid is less influential, as this is not a fraction produced in large quantities in steam reforming processes. In the absence of a sorbent (CaO/m_{org} = 0 g min/g), liquid formation is only significant at low temperatures (400–500 °C) and using a low W_{cat}/m_{org} ratio (4 g min/g). Under such conditions, increasing the temperature drops the C yield to liquid due to the helpful temperature impact on gas formation via reforming [23,44]. On the contrary, for a high amount of sorbent (CaO/m_{org} = 85 g min/g), liquid production is only promoted at low temperatures (400–500 °C) with a high proportion of catalyst (W_{cat}/m_{org} ratio of 16 g min/g). As discussed earlier, increasing the amount of catalyst at low temperatures can aid in the gasification/reforming of the solid residues, forming intermediate liquid products at low temperatures. Consequently, increasing the temperature decreases the C yield to liquid, and negligible C yields to liquid are obtained at temperatures between 500 and 700 °C.

3.4.2. Gas phase volumetric composition

The gas phase primarily comprises a mixture of H_2 and CO_2, whose volumetric compositions vary by 63–100 vol% and 0–35 vol%, along with small amounts of CO (0–3 vol%) and CH_4 (0–13 vol%). The cause-effect Pareto test (Table 5) reveals that the temperature, followed by the CaO/m_{org} and W_{cat}/m_{org} ratios, is the processing parameter exerting the most significant influence on the relative amounts of H_2, CO and CO_2. Besides, different interactions between the temperature and the CaO/m_{org} and W_{cat}/m_{org} ratios also impact the proportion of these gases. Contrarily, the relative amount of CH_4 is mainly influenced by the CaO/m_{org} and W_{cat}/m_{org} ratios, with the temperature exerting a less marked impact. It is also important to note that similar coefficients but with opposite signs were obtained in the ANOVA models for the volumetric concentrations of H_2 and CO_2. This indicates that diminishments in those of the latter account for increases in the former and *vice versa*. Fig. 7 plots the influences on the reaction temperature and W_{cat}/m_{org} and CaO/m_{org} ratios on the volumetric composition of the gas phase. Fig. 7 a, d, g and j shows the influence of the temperature on the relative amounts of H_2, CO_2, CO and CH_4 as a function of the amount of CaO (CaO/m_{org} = 0 and 85 g min/g), with a W_{cat}/m_{org} ratio of 4 g min/g. Additionally, Fig. 6 b/e/h/k and c/f/i/l plot these influences for a W_{cat}/m_{org} ratio of 10 and 16 g min/g, respectively.

The impact of the temperature on the volumetric composition of the gas depends on the relative amounts of catalyst and sorbent (W_{cat}/m_{org} and CaO/m_{org} ratios) used. In the absence of a sorbent (CaO/m_{org} = 0 g min/g), the impacts of the temperature or W_{cat}/m_{org} ratio are not important. Regardless of these variables, the gas primarily comprises c. a., 70 vol% H_2 and 30 vol% CO_2, with minimal, unimportant practical variations. Likewise, the proportions of CO and CH_4 in the gas are meagre (< 5 vol%). Upsurging the relative amount of sorbent alters the impact of the temperature and catalyst amount on the gas composition. Notably, the detailed influence of increasing the amount of sorbent (CaO/m_{org}) from 0 to 85 g min/g depends on the temperature and the relative amount of catalyst. With a W_{cat}/m_{org} of 4 g min/g, such development is controlled by the process temperature. Between 400 and 600 °C, increasing the CaO/m_{org} ratio from 0 to 85 g min/g leads to an extensive rise in the relative amount of H_2 and a diminishment in the proportion of CO_2 in the gas. This variation is accounted for by the sorbent capacity of the calcinated eggshells (CaO), transforming the CO_2 to $CaCO_3$ [24–27]. The temperature directs this adsorption capacity, which is promoted at low temperatures due to the exothermic nature of such a transformation [24–27]. At high temperatures (650–700 °C), an increase in the relative amount of sorbent diminishes the volumetric concentration of H_2 and upsurges the proportion of CH_4 in the gas. These results indicate that CaO might have a dual influence on reforming; i.e., it can be an excellent sorbent for capturing CO_2 at low temperatures [24–27], but it can also exert a catalytic impact on the methanation reaction to produce CH_4 at high temperatures when the adsorption process is not thermodynamically promoted [50]. This latter seems to modify the equilibria of the reforming processes as the relative amount of H_2 obtained is lower than that attained in the absence of a sorbent, and that is thermodynamically expected. This alternation aligns with the increase observed in the proportion of CH_4 in the gas, with this latter being superior to the experimental and thermodynamic values without a sorbent.

The impact of the relative amount of catalyst in the presence of the greatest amount of sorbent (CaO/m_{org} = 85 g min/g) depends on the temperature. At low temperatures (400–500 °C), increasing the W_{cat}/m_{org} ratio from 4 to 16 g min/g drops the proportion of H_2 at the expense of the relative amount of CO_2 in the gas (Fig. 7 a/d/g/j vs b/e/h/k vs c/f/i/l). Such an increment in the CO_2 volumetric concentration relates to promoting catalyst impact on the gasification of non-vaporised carbonaceous matter [23,44]. Consequently, the gas contains more CO_2 than that the amount of CaO in the bed can absorb under such conditions. Contrarily, at high temperatures (620–700 °C), such an increase in the relative amount of catalyst increases the proportion of H_2 at the expense of the relative amount of CH_4 in the gas. Therefore, increasing the amount of catalyst might hinder the catalytic ability of CaO to promote the methanation reaction. This intensifies the reforming and water gas shift reactions yielding H_2 and CO_2, decreasing the development of the methanation reaction catalysed by CaO at a high temperature [50]. As a result, the increments occurring in the concentration of CH_4 in the gas from 620 to 700 °C decrease progressively with increasing the W_{cat}/m_{org} ratio (Fig. 7 j vs k vs l). As a result of these developments, a gas with a very high H_2 proportion (> 95 vol%) can be obtained in the presence of the greatest amount of calcinated eggshells (CaO/m_{org} = 85 g min/g) regardless of the amount of catalyst used. Upsurging the temperature from 400 to 550 °C does not noticeably modify the volumetric composition of the gas. On the contrary, the relative amount of H_2 drops at the expense of that of CO_2 between 550 and 700 °C due to the less efficient adsorption capability of CaO at higher than lower temperatures, with

such a diminishment being accounted for by the exothermicity of the carbonation reaction [24–27].

3.5. SESR of the aqueous fraction: Adsorption capability of the eggshell-derived CaO

Elemental analysis was conducted on the spent solid to determine the C_{ad}/C_{max} ratio, representing the ratio between the C in the solid and the maximum C in the solid if all CaO had been converted to $CaCO_3$. This ratio shifted from 0 to 81 % depending on the processing conditions and relates well to the colour of the spent solid, i.e., white for C_{ad}/C_{max} low ratios (< 5 %), where the solid mostly comprises CaO and grey for high C_{ad}/C_{max} ratios (> 70 %), with the solid containing a high proportion of $CaCO_3$. The C_{ad}/C_{max} ratio was also related to the operating conditions using the ANOVA and the cause-effect Pareto test (Table 6). This latter analysis shows that reforming temperature, followed by the CaO/m_{org} ratio, is the processing parameter impacting the C_{ad}/C_{max} ratio most significantly.

Fig. 8 summarises the impact of the processing conditions and significant interactions on the C_{ad}/C_{max} ratio. In particular, Fig. 8 a, b and c plots the influence of the CaO/m_{org} ratio as a function of the W_{cat}/m_{org} ratio (4 and 16 g min/g) at 400, 550 and 700 °C, respectively. In the absence of sorbent (CaO/m_{org} = 0 g min/g), the C_{ad}/C_{max} ratio is null as the carbonation reaction does not occur. Regardless of the processing conditions (temperature or relative amount of catalyst), a first increment in the relative amount of sorbent (CaO/m_{org} ratio) up to around 50 g min/g leads to an increment in the C_{ad}/C_{max} ratio, as the amount of CaO that can be converted to $CaCO_3$ increases progressively. However, a subsequent increment to 85 g min/g drops the C_{ad}/C_{max} ratio as there is an excess of sorbent. This translates into an increment in the C_{max} value without modifying the C_{ad}, resulting in a progressive drop in the C_{ad}/C_{max} ratio. Notably, the maximum amount of CO_2 produced during the first 30 min of the reaction (considering the liquid flow rate and the concentration of organics in the aqueous effluent) is 0.89 g CO_2. Such an amount of CO_2 can theoretically produce 2 g of $CaCO_3$ during the reaction with 1.13 g of CaO, equivalent to a CaO/m_{org} ratio of 48 min g/min.

Besides, the effective conversion of CaO to $CaCO_3$ depends on the temperature and the relative amount of catalyst used. An increase in the temperature between 400 and 550 °C upsurges the C_{ad}/C_{max} ratio (Fig. 8 a vs b), regardless of the relative amounts of catalyst or sorbent used. Conversely, a subsequent increment from this temperature to 700 °C drops the C_{ad}/C_{max} ratio (Fig. 8 b vs c). Such variations have thermodynamics and kinetics origins, with more marked variations for greater than lesser sorbent amounts. The CO_2 capture via the chemical transformation of CaO to $CaCO_3$ is an exothermic process favoured at low temperatures [24–27]. Between 400 and 550–600 °C, such a transformation is thermodynamically favoured, and increasing the temperature kinetically impacts the reaction rate, translating into an increment in the C_{ad}/C_{max} ratio. Conversely, between 550–700 °C, the negative thermodynamic influence of the temperature is higher than the positive kinetic impact. This leads to a decrease in the development of the carbonation reaction to capture CO_2, dropping the C_{ad}/C_{max} ratio.

Likewise, the impact of the relative amount of catalyst (W_{cat}/m_{org} ratio) primarily depends on the amount of sorbent (CaO/m_{org}) used. When a low amount of sorbent is used (CaO/m_{org} between 0 and 30 g min/g), the impact of the catalyst on the W_{cat}/m_{org} ratio is insignificant. However, when the process is conducted with greater amounts of CaO (calcined eggshells), the relative amount of catalyst influences the adsorption capabilities of the calcined eggshells. For CaO/m_{org} ratios between ca. 40 and 85 g min/g, increasing the W_{cat}/m_{org} ratio from 4 to 16 g min/g leads to increases in the C_{ad}/C_{max} ratio, regardless of the temperature. Such increments are related to the beneficial effect of the catalyst on the reforming process, increasing the relative amount of CO_2 in the gas phase and its formation reaction rate, which translates into an increment in the C_{ad}/C_{max} ratio.

3.6. SESR of the aqueous fraction: Process mechanism

Fig. 9 shows a proposed process mechanism considering the information gathered and discussed in previous sections. The process comprises three tandem steps, i.e., i.) atomisation and vaporisation, ii.) reaction and CO_2 capture (carbonation) and iii.) gas–liquid separation. In the first step, the aqueous fraction, containing a mixture of organic compounds ($C_xH_yO_z$) in water, is fed into the reactor, where its vaporisation takes place prior to reaching the catalytic bed, leading to gas (vaporised aqueous fraction and steam) formation. The temperature of this reactor zone is lower than that of the catalytic bed, which can result in solid matter formation (char) due to incomplete vaporisation. This latter process is intensified at lower reaction temperatures, as the lower the reaction temperature, the lower the temperature of the atomisation and vaporisation zone. Other phenomena can occur within this zone, altering the C distribution between the gas and solid phases. One is the steam gasification of the carbon matter (char) deposited in this area due to the high water-to-carbon ratio of the feedstock. Another is liquid–solid interactions during the atomisation process, as the liquid drops entering the reactor can crash with solid particles (char) before vaporisation. Such an interaction leads to a less efficient liquid atomisation, which increases the liquid drop size and diminishes the liquid vaporisation rate [51]. As a result, the vaporisation process is less efficient and solid matter formation increases [23,44].

In the second step, the vaporised aqueous fraction and steam (H_2O) reach the catalytic bed, which contains a homogeneous mixture of catalyst (Ni-Co/Al-Mg) and CaO. The catalyst comprises Ni-Co_x species, resulting in oxygen vacant sites and labile species on the support, favouring steam reforming and carbon intermediates gasification, diminishing catalyst deactivation [40]. As a result, the vaporised aqueous fraction is converted into a mixture of H_2 and carbon-containing gases, primarily CO_2, with small amounts of CO and CH_4, depending on the reaction temperature. In this step, CO_2 reacts with the CaO in the bed as soon as it is produced via carbonation. The carbonation reaction of CaO, leading to the formation of $CaCO_3$, takes place in two steps [25,27]. Initially, only a small amount of $CaCO_3$ is formed, covering a small area of the unreacted CaO, with the rest exposed to CO_2. Secondly, the CaO surface is covered wholly by $CaCO_3$, hindering direct contact with CO_2. At this point, the carbonatation rate slows (rate-limiting step) as CO_2 needs to diffuse through the outer $CaCO_3$ layer to continue the reaction. The carbonation reaction reduces the CO_2 partial

Table 6
Relative influence of the processing conditions on the C_{ad}/C_{max} ratio.

	R^2	Ind.	A	B	C	AB	AC	BC	A^2	B^2	C^2	ABC	A^2B	A^2C	AB^2
C_{ad}/C_{max} (%)	0.99	74.79	−17.23 (56)	4.73 (4)	40.06 (18)	n.s.	− 5.45 (4)	5.23 (3)	−14.63 (18)	−5.88 (8)	−34.79 (13)	n.s.	n.s.	−20.57 (6)	11.77 (4)

A = Temperature, B = $W_{cat}/morg$, C = $CaO/m_{org,}$ n.s. = not significant with 95 % confidence.
Response = Ind. + Coefficient A·A + Coefficient B·B + Coefficient C·C + Coefficient AB·A·B + Coefficient AB·A·B + Coefficient BC·B·C + Coefficient A^2·A^2 + Coefficient B^2·B^2 + Coefficient C^2·C^2 + Coefficient ABC·A·B·C + Coefficient A^2B·A^2·B + Coefficient A^2B·A^2·B + Coefficient AB^2·A·B^2 + Coefficient A^2B^2·A^2·B^2.
Standardised codec formula: all operating variables vary between −1 and + 1. Numbers in brackets show the relative influence (%) of each factor on the response variable.

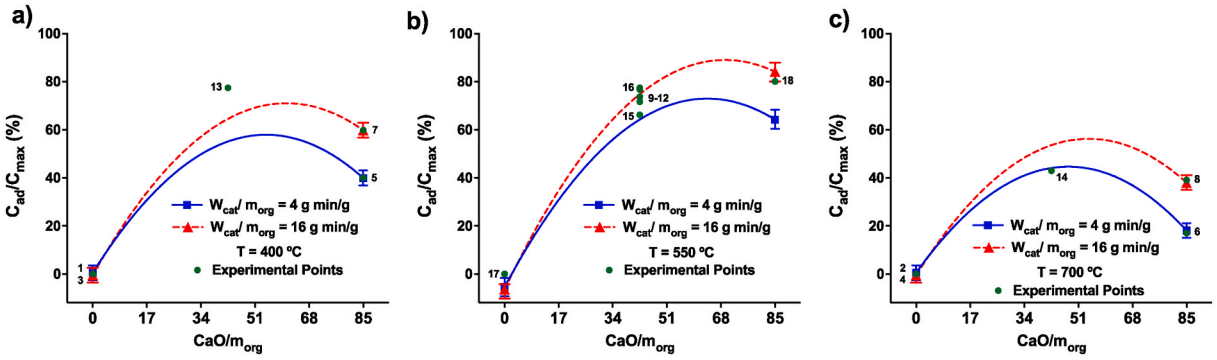

Fig. 8. Effect of the processing conditions (temperature, W_{cat}/m_{org} and CaO/m_{org} ratios) on the C_{ad}/C_{max} ratio.

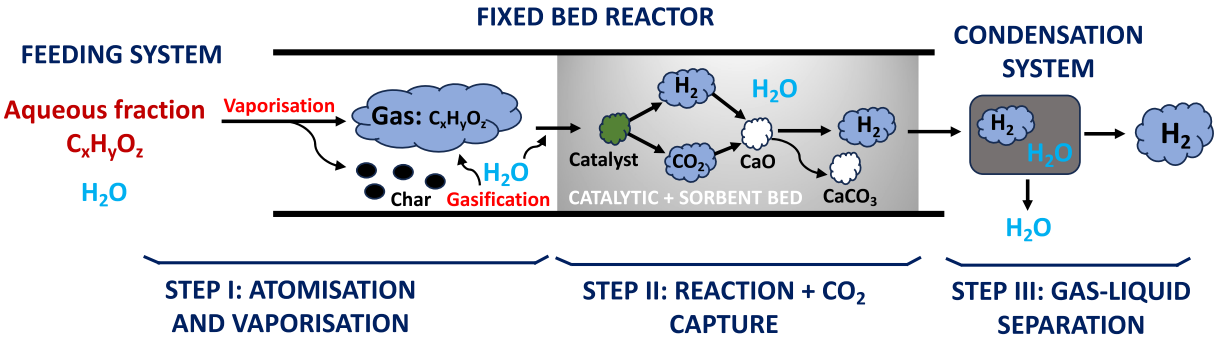

Fig. 9. Sorption-enhanced steam reforming (SESR) detailed process mechanism.

pressure in the gas mixture, which shifts the equilibrium of the water gas shift reaction ($CO + H_2O = CO_2 + H_2$) towards the production of H_2 [24–27]. This leads to a decrease in the partial pressure of CO, which shifts the CH_4 reforming reaction ($CH_4 + H_2O = CO + 3H_2$) towards the production of H_2, increasing the relative amount of H_2 in the gas and, simultaneously decreasing the amounts of CO and CH_4 [24–27]. As a result, the gas phase contains a very high concentration of H_2. In the third step, the temperature of the gaseous mixture decreases, which allows for the separation of permanent gases (mostly H_2 with a low amount of C-containing gases) and vapours (H_2O).

3.7. Process optimisation

The process has been optimised to produce a highly pure H_2 gas from the SESR of the almond hull-derived aqueous fraction using the empirical formulae developed with the ANOVA of the results. The actual, adjusted, and predicted (R^2, $R^2_{adjusted}$, and $R^2_{predicted}$) regression coefficients in the model surpass 0.95, with significant signal-to-noise ratios (> 4) and insignificant lack-of-fit tests (p-value > 0.05) in all models. As such, these models can be effectively used to predict accurately. To accomplish this goal, the C yields to gas and solid have been maximised, with the C yield to liquid minimised to guarantee gas production and boost the effective capture of CO_2 via the transformation of CaO into $CaCO_3$. Simultaneously, the relative amounts of H_2 and CO_2 in the gas have been maximised and minimised, respectively, with the C_{ad}/C_{max} ratio being maximised to promote CO_2 capture and increase the H_2 purity of the gas. All the constraints in the optimisation were given relative importance (from the last 1 to the most important 5) to ensure a compromise solution that satisfies every criterion. Table 7 lists the optimisation criteria and the results attained.

Process optimisation shows that the aqueous effluent produced during the HTT of almond hulls can be converted into a highly pure H_2 gas (95 vol%) by SESR at 500 °C using a W_{cat}/m_{org} ratio of 9 g min/g and a relative amount of calcinated eggshells (CaO/m_{org}) of 70 g min/g. This

Table 7
Theoretical optimisation: restrictions and optimal processing parameters.

	Objective	Solution
Temperature (°C)		501
W_{cat}/m_{org} (g min/g)		9.4
CaO/m_{org} (g min/g)		70
Overall yields		
C yield to gas (%)	Maximise (3)	24.82 ± 3,39
C yield to solid (%)	Maximise (3)	74.91 ± 3.4
C yield to liquid (%)	Minimise (3)	0.27 ± 0.86
Composition of the gas		
H_2 (vol.%)	Maximise (5)	94.98 ± 0.62
CO_2 (vol.%)	Minimise (5)	5.02 ± 0.73
CO (vol.%)	Minimise (5)	0 ± 0.01
CH_4 (vol.%)	Minimise (5)	0 ± 0.01
Adsorption capacity		
C_{ad}/C_{max}	Maximise (4)	88.98 ± 2.32
H_2 Production		
H_2 yield (g/g org)*		0.12 ± 0.005

* Codec ANOVA model for the H_2 yield (g/g org) = 0.1199 + 0.0411 A + 0.0272C – 0.0106 AB – 0.031 AC – 0.037 B^2 – 0.0199 C^2 – 0.0143 ABC + 0.09 A^2B – 0.0385 A_2C – 0.0241 AB^2. A = Temperature, B = W_{cat}/m_{org}, C = CaO/m_{org}. Standardised codec formula: all operating variables vary between −1 and + 1.

reforming temperature is significantly lower than the typical optimum temperatures reported in the literature for steam reforming (between 600 and 700 °C). Such a reduction might be accounted for by the fact that the sorption-enhanced steam reforming process couples the endothermic H_2 production with the exothermic nature of the carbonation reaction, which results in a decrease in the processing temperature. Under such conditions, the C yield to liquid is negligible, contributing to efficient management of the original aqueous effluent, and the adsorption capability of the calcined eggshells is exceptionally high, with a C_{ad}/C_{max} ratio of ca. 90 %. Additionally, H_2 production is substantially high, with a H_2 yield of 0.12 g of H_2/g of organics. Such a value is slightly higher than the thermodynamic H_2 production (0.1174 g of H_2/

g of organics, Table S.2), as CO_2 capture modifies the equilibrium of the system as described above. However, this value equals the maximum stoichiometric H_2 production (0.12 g of H_2/g of organics) that could be attained, considering the chemical composition of the aqueous fraction. As a result, the high C yield to solid derived from the high CO_2 capture, which transformed the vast amount of the sorbent (CaO) into $CaCO_3$. Thus, the C yield to solid corresponds to $CaCO_3$ formation, which indicates that vaporisation took place efficiently and the vast amount of the C content of the aqueous fraction was vaporised efficiently, converted to CO_2 and then captured as $CaCO_3$. These values were experimentally corroborated without significant differences between predicted and experimental data (p-value > 0.95). Thus, these results demonstrate the practical viability of our 'sorption-egg-hanced' approach, i.e., using calcined eggshells (CaO) as the sorbent to develop more sustainable sorption-enhanced reforming processes to produce H_2-rich streams from biomass-derived aqueous effluents.

The experimental results of this work demonstrate the excellent performance of the catalyst in combination with CaO produced from eggshells, as thermodynamic yields and gas compositions were achieved. As for future work, the natural subsequent step might be the development of bifunctional materials joining catalytic and sorption capabilities using a sorbent and a catalyst that work well simultaneously. Thus, future research will focus on producing active bifunctional materials, i.e., exploring the development of Ni/CaO-eggshell-derived catalysts. Combining both phenomena (catalysis and adsorption) will intensify the process, allowing fuller contact between the catalytic and adsorption domains and decreasing heat and mass transfer limitations. This research is new and challenging due to the possible irreversible interactions between the catalyst, sorbent and support.

4. Conclusions

This work has addressed a novel 'sorption-egg-hanced' reforming approach to producing high-pure H_2 from an aqueous fraction yielded during the hydrothermal treatment of almond hulls. The reforming process was conducted over a Ni-based catalyst with excellent reforming capabilities, with the sorption-enhanced step being incorporated in the process using eggshells as a natural source of Ca to produce the CaO used as the sorbent. The physicochemical characterisation of the eggshells revealed that they were mostly $CaCO_3$, effectively converted to CaO by calcination at 900 °C for 3 h. The reforming conditions significantly influenced the process, with the temperature and the relative amount of catalyst primarily directing the overall product distribution. The former favoured gas formation, preventing solid production due to its positive impact on the vaporisation of the feed and offsetting the overall endothermicity of the reforming process, while the latter allowed for lower temperatures to be used. Additionally, the relative amount of calcined eggshells (CaO/ organic mass flow rate) significantly impacted the gas composition, with increments noted in the relative amount of H_2 at the expense of C-derived gases (CO_2, CO and CH_4) as the amount of sorbent increased. This sorbent capability was temperature-ruled due to a mix of impacts from thermodynamics and kinetics. The exothermicity of the carbonation reaction responsible for an effective CO_2 capture allowed higher H_2 purities at temperatures lower than 550 °C, with the temperature kinetically promoting the carbonisation reaction within 400 and 550 °C. However, the negative thermodynamic impact of the temperature surpassed its positive kinetic influence at temperatures higher than 550 °C, decreasing CO_2 capture and H_2 purity. Process optimisation revealed that operating at 500 °C, using a W_{cat}/m_{org} ratio of 9 g min/g with CaO/m_{org} ratio of 70 g min/g allowed transforming the almond hull-derived aqueous effluent into a gas with a highly high H_2 content ($>$ 95 vol%). Such conditions maximised the adsorption capabilities of the calcined eggshells, capturing up to 90 % of the CO_2 produced, which resulted in a very high H_2 production (0.12 g of H_2/g of organics, equivalent to the maximum stoichiometric value). These promising features demonstrate the viability of our 'sorption-egg-hanced' approach to producing H_2-rich streams from biomass-derived aqueous effluents, promoting process intensification with H_2 production and CO_2 capture in a single unit, avoiding further downstream processes.

CRediT authorship contribution statement

Javier Remón: Writing – original draft, Supervision, Resources, Project administration, Methodology, Investigation, Funding acquisition, Formal analysis, Data curation, Conceptualization. **Edurne Val-Planells:** Investigation, Formal analysis, Data curation. **Avtar S. Matharu:** Writing – review & editing, Validation, Investigation. **Lucía García:** Writing – review & editing, Validation, Resources, Investigation. **Jesús Arauzo:** Writing – review & editing, Validation, Resources, Investigation.

Declaration of competing interest

The authors declare that they have no known competing financial interests or personal relationships that could have appeared to influence the work reported in this paper.

Acknowledgements

The authors would like to acknowledge the Aragón Government (Research Group Reference T22_23R) for providing frame support and using Servicio General de Apoyo a la Investigación-SAI, Universidad de Zaragoza. Besides, Javier Remón thanks MCIN/AEI/10.13039/501100011033 and the European Union «NextGenerationEU»/PRTR» for the Ramón y Cajal Fellowship (RYC2021-033368-I) awarded. We thank Rua Restauración (https://ruarestauracion.com) for providing the eggshells used in this work.

Appendix A. Supplementary data

Supplementary data to this article can be found online at https://doi.org/10.1016/j.cej.2025.163524.

Data availability

Data will be made available on request.

References

[1] B. Liu, D. Rajagopal, Life-cycle energy and climate benefits of energy recovery from wastes and biomass residues in the United States, Nat. Energy 4 (8) (2019) 700–708, https://doi.org/10.1038/s41560-019-0430-2.
[2] G. Semieniuk, P.B. Holden, J.-F. Mercure, P. Salas, H. Pollitt, K. Jobson, P. Vercoulen, U. Chewpreecha, N.R. Edwards, J.E. Viñuales, Stranded fossil-fuel assets translate to major losses for investors in advanced economies, Nat. Clim. Chang. 12 (6) (2022) 532–538, https://doi.org/10.1038/s41558-022-01356-y.
[3] A. Ariza, M. Lengaigne, C. Menkes, A. Lebourges-Dhaussy, A. Receveur, T. Gorgues, J. Habasque, M. Gutiérrez, O. Maury, A. Bertrand, Global decline of pelagic fauna in a warmer ocean, Nat. Clim. Chang. 12 (10) (2022) 928–934, https://doi.org/10.1038/s41558-022-01479-2.
[4] M.D. Staples, R. Malina, S.R.H. Barrett, The limits of bioenergy for mitigating global life-cycle greenhouse gas emissions from fossil fuels, Nat. Energy 2 (2) (2017) 16202, https://doi.org/10.1038/nenergy.2016.202.
[5] A.C. Opia, M.K.B.A. Hamid, S. Syahrullail, A.B.A. Rahim, C.A.N. Johnson, Biomass as a potential source of sustainable fuel, chemical and tribological materials – Overview, Materials Today: Proceedings 39 (2021) 922-928. https://doi.org/10.1016/j.matpr.2020.04.045.
[6] S. Dutta, I.K.M. Yu, J. Fan, J.H. Clark, D.C.W. Tsang, Critical factors for levulinic acid production from starch-rich food waste: solvent effects, reaction pressure, and phase separation, Green Chem. 24 (1) (2022) 163–175, https://doi.org/10.1039/d1gc01948a.
[7] T.M.W. Mak, X. Xiong, D.C.W. Tsang, I.K.M. Yu, C.S. Poon, Sustainable food waste management towards circular bioeconomy: Policy review, limitations and opportunities, Bioresour. Technol. 297 (2020) 122497, https://doi.org/10.1016/j.biortech.2019.122497.
[8] A.J. Esfahlan, R. Jamei, R.J. Esfahlan, The importance of almond (Prunus amygdalus L.) and its by-products, Food Chem. 120(2) (2010) 349-360. https://doi.org/10.1016/j.foodchem.2009.09.063.

[9] J. Remon, R. Sevilla-Gasca, E. Frecha, J.L. Pinilla, I. Suelves, Direct conversion of almond waste into value-added liquids using carbon-neutral catalysts: Hydrothermal hydrogenation of almond hulls over a Ru/CNF catalyst, Sci. Total Environ. (2022) 154044, https://doi.org/10.1016/j.scitotenv.2022.154044.
[10] J. Remón, J. Latorre-Viu, A.S. Matharu, J.L. Pinilla, I. Suelves, Analysis and optimisation of a novel 'almond-refinery' concept: Simultaneous production of biofuels and value-added chemicals by hydrothermal treatment of almond hulls, Sci. Total Environ. 765 (2021) 142671, https://doi.org/10.1016/j.scitotenv.2020.142671.
[11] Y. Gao, J. Remón, A.S. Matharu, Microwave-assisted hydrothermal treatments for biomass valorisation: a critical review, Green Chem. 23 (10) (2021) 3502–3525, https://doi.org/10.1039/d1gc00623a.
[12] M. Kumar, A. Olajire Oyedun, A. Kumar, A review on the current status of various hydrothermal technologies on biomass feedstock, Renew Sust Energ Rev 81 (2018) 1742–1770, https://doi.org/10.1016/j.rser.2017.05.270.
[13] A. Dimitriadis, S. Bezergianni, Hydrothermal liquefaction of various biomass and waste feedstocks for biocrude production: A state of the art review, Renew. Sust. Energ. Rev. 68 (2017) 113–125, https://doi.org/10.1016/j.rser.2016.09.120.
[14] J.A. Okolie, E.I. Epelle, S. Nanda, D. Castello, A.K. Dalai, J.A. Kozinski, Modeling and process optimization of hydrothermal gasification for hydrogen production: A comprehensive review, J. Supercrit. Fluids 173 (2021), https://doi.org/10.1016/j.supflu.2021.105199.
[15] K. Sharma, D. Castello, M.S. Haider, T.H. Pedersen, L.A. Rosendahl, Continuous co-processing of HTL bio-oil with renewable feed for drop-in biofuels production for sustainable refinery processes, Fuel 306 (2021), https://doi.org/10.1016/j.fuel.2021.121579.
[16] D.C. Elliott, P. Biller, A.B. Ross, A.J. Schmidt, S.B. Jones, Hydrothermal liquefaction of biomass: developments from batch to continuous process, Bioresour. Technol. 178 (2015) 147–156, https://doi.org/10.1016/j.biortech.2014.09.132.
[17] S.S. Toor, L. Rosendahl, A. Rudolf, Hydrothermal liquefaction of biomass: A review of subcritical water technologies, Energy 36 (5) (2011) 2328–2342, https://doi.org/10.1016/j.energy.2011.03.013.
[18] J. Remón, F. Ravaglio-Pasquini, L. Pedraza-Segura, P. Arcelus-Arrillaga, I. Suelves, J.L. Pinilla, Caffeinating the biofuels market: Effect of the processing conditions during the production of biofuels and high-value chemicals by hydrothermal treatment of residual coffee pulp, J. Clean. Prod. 302 (2021), https://doi.org/10.1016/j.jclepro.2021.127008.
[19] S. Leng, L. Leng, L. Chen, J. Chen, J. Chen, W. Zhou, The effect of aqueous phase recirculation on hydrothermal liquefaction/carbonization of biomass: A review, Bioresour. Technol. 318 (2020) 124081, https://doi.org/10.1016/j.biortech.2020.124081.
[20] P. Das, M. AbdulQuadir, M. Thaher, S. Khan, A.K. Chaudhary, H. Al-Jabri, A feasibility study of utilizing hydrothermal liquefaction derived aqueous phase as nutrients for semi-continuous cultivation of Tetraselmis sp, Bioresour. Technol. 295 (2020) 122310, https://doi.org/10.1016/j.biortech.2019.122310.
[21] F. Marrakchi, S. Sohail Toor, A. Haaning Nielsen, T. Helmer Pedersen, L. Aistrup Rosendahl, Bio-crude oils production from wheat stem under subcritical water conditions and batch adsorption of post-hydrothermal liquefaction aqueous phase onto activated hydrochars, Chem. Eng. J. 452 (2023) 139293, https://doi.org/10.1016/j.cej.2022.139293.
[22] A. Aho, M. Alvear, J. Ahola, J. Kangas, J. Tanskanen, I. Simakova, J.L. Santos, K. Eranen, T. Salmi, D.Y. Murzin, H. Grenman, Aqueous phase reforming of birch and pine hemicellulose hydrolysates, Bioresour. Technol. 348 (2022) 126809, https://doi.org/10.1016/j.biortech.2022.126809.
[23] J. Remón, L. García, J. Arauzo, Cheese whey management by catalytic steam reforming and aqueous phase reforming, Fuel Process. Technol. 154 (2016) 66–81, https://doi.org/10.1016/j.fuproc.2016.08.012.
[24] S. Ayalur Chattanathan, S. Adhikari, N. Abdoulmoumine, A review on current status of hydrogen production from bio-oil, Renew Sust Energ Rev 16(5) (2012) 2366-2372. https://doi.org/10.1016/j.rser.2012.01.051.
[25] S. Guo, Y. Zhang, L. Liu, Sorption enhanced steam reforming of biomass-based feedstocks: Towards sustainable hydrogen evolution, Chem. Eng. J. 485 (2024), https://doi.org/10.1016/j.cej.2024.149760.
[26] Y. Li, L. Wu, Q. Xu, Z. Li, Hydrogen-rich gas production from sorption-enhanced sludge gasification using CaO-based biochar derived from crab shell as a CO2 sorbent, J. Mater. Cycles Waste Manage. 24 (6) (2022) 2353–2364, https://doi.org/10.1007/s10163-022-01480-z.
[27] Y. Wang, M.Z. Memon, M.A. Seelro, W. Fu, Y. Gao, Y. Dong, G. Ji, A review of CO2 sorbents for promoting hydrogen production in the sorption-enhanced steam reforming process, Int. J. Hydrogen Energy 46 (45) (2021) 23358–23379, https://doi.org/10.1016/j.ijhydene.2021.01.206.
[28] L. Landa, A. Remiro, J. Valecillos, B. Valle, S. Sun, C. Wu, J. Bilbao, A.G. Gayubo, Sorption enhanced steam reforming (SESR) of raw bio-oil with Ni based catalysts: Effect of sorbent type, catalyst support and sorbent/catalyst mass ratio, Fuel Process. Technol. 247 (2023), https://doi.org/10.1016/j.fuproc.2023.107799.
[29] A. Mostafa, I. Rapone, A. Bosetti, M.C. Romano, A. Beretta, G. Groppi, Sustainable Hydrogen Production via Sorption Enhanced Reforming of Complex Biorefinery Side Streams in a Fixed Bed Adiabatic Reactor, Ind. Eng. Chem. Res. 62 (39) (2023) 15884–15896, https://doi.org/10.1021/acs.iecr.3c02401.
[30] M. Imani, M. Tahmasebpoor, P.E. Sánchez-Jiménez, J.M. Valverde, V. Moreno, Improvement in cyclic CO2 capture performance and fluidization behavior of eggshell-derived CaCO3 particles modified with acetic acid used in calcium looping process, J. CO2 Util. 65 (2022), https://doi.org/10.1016/j.jcou.2022.102207.
[31] T.E. Odetoye, J.O. Agu, E.O. Ajala, Biodiesel production from poultry wastes: Waste chicken fat and eggshell, J. Environ. Chem. Eng 9 (4) (2021), https://doi.org/10.1016/j.jece.2021.105654.
[32] M. Queirós, M. Bezerra, J. Feitosa, Composite Superabsorbent Hydrogel of Acrylic Copolymer and Eggshell: Effect of Biofiller Addition, J. Braz. Chem. Soc. (2017), https://doi.org/10.21577/0103-5053.20170046.
[33] D. Yang, J. Zhao, W. Ahmad, M. Nasir Amin, F. Aslam, K. Khan, A. Ahmad, Potential use of waste eggshells in cement-based materials: A bibliographic analysis and review of the material properties, Constr Build Mater 344 (2022), https://doi.org/10.1016/j.conbuildmat.2022.128143.
[34] M. Ayesha, A.H. Khoja, F.A. Butt, U. Sikandar, A.H. Javed, S.R. Naqvi, I.u. din, M. T. Mehran, Sorption enhanced steam reforming of methane over waste-derived CaO promoted MgNiAl hydrotalcite catalyst for sustainable H2 production, J. Environ. Chem. Eng 10 (3) (2022), https://doi.org/10.1016/j.jece.2022.107651.
[35] L. Habte, N. Shiferaw, D. Mulatu, T. Thenepalli, R. Chilakala, J. Ahn, Synthesis of Nano-Calcium Oxide from Waste Eggshell by Sol-Gel Method, Sustainability 11 (11) (2019), https://doi.org/10.3390/su11113196.
[36] J. Remón, G. Zapata, L. Oriol, J.L. Pinilla, I. Suelves, A novel 'sea-thermal', synergistic co-valorisation approach for biofuels production from unavoidable food waste (almond hulls) and plastic residues (disposable face masks), Chem. Eng. J. 449 (2022), https://doi.org/10.1016/j.cej.2022.137810.
[37] Y. Zhou, J. Remón, J. Gracia, Z. Jiang, J.L. Pinilla, C. Hu, I. Suelves, Toward developing more sustainable marine biorefineries: A novel 'sea-thermal' process for biofuels production from microalgae, Energy Convers. Manage. 270 (2022), https://doi.org/10.1016/j.enconman.2022.116201.
[38] S.A. Channiwala, P.P. Parikh, A unified correlation for estimating HHV of solid, liquid and gaseous fuels, Fuel 81 (8) (2002) 1051–1063, https://doi.org/10.1016/s0016-2361(01)00131-4.
[39] J. Remón, F. Santomauro, C.J. Chuck, A.S. Matharu, J.H. Clark, Production of fermentable species by microwave-assisted hydrothermal treatment of biomass carbohydrates: reactivity and fermentability assessments, Green Chem. 20 (19) (2018) 4507–4520, https://doi.org/10.1039/c8gc02182a.
[40] J. Remón, J.A. Medrano, F. Bimbela, L. García, J. Arauzo, Ni/Al–Mg–O solids modified with Co or Cu for the catalytic steam reforming of bio-oil, Appl. Catal., B 132-133 (2013) 433-444. https://doi.org/10.1016/j.apcatb.2012.12.015.
[41] J. Remón, C. Jarauta-Córdoba, L. García, J. Arauzo, Analysis and optimisation of H2 production from crude glycerol by steam reforming using a novel two step process, Fuel Process. Technol. 145 (2016) 130–147, https://doi.org/10.1016/j.fuproc.2016.01.035.
[42] J. Remón, F. Broust, J. Valette, Y. Chhiti, I. Alava, A.R. Fernandez-Akarregi, J. Arauzo, L. Garcia, Production of a hydrogen-rich gas from fast pyrolysis bio-oils: Comparison between homogeneous and catalytic steam reforming routes, Int. J. Hydrogen Energy 39 (1) (2014) 171–182, https://doi.org/10.1016/j.ijhydene.2013.10.025.
[43] J. Remón, F. Broust, G. Volle, L. García, J. Arauzo, Hydrogen production from pine and poplar bio-oils by catalytic steam reforming. Influence of the bio-oil composition on the process, Int. J. Hydrogen Energy 40(16) (2015) 5593-5608. https://doi.org/10.1016/j.ijhydene.2015.02.117.
[44] J. Remón, M. Laseca, L. García, J. Arauzo, Hydrogen production from cheese whey by catalytic steam reforming: Preliminary study using lactose as a model compound, Energy Convers. Manage. 114 (2016) 122–141, https://doi.org/10.1016/j.enconman.2016.02.009.
[45] J. Remón, P. Arcelus-Arrillaga, L. García, J. Arauzo, Production of gaseous and liquid bio-fuels from the upgrading of lignocellulosic bio-oil in sub- and supercritical water: Effect of operating conditions on the process, Energy Convers. Manage. 119 (2016) 14–36, https://doi.org/10.1016/j.enconman.2016.04.010.
[46] G. Busca, C. Resini, Vibrational Spectroscopy for the Analysis of Geological and Inorganic Materials, Encyclopedia of Analytical Chemistry. https://doi.org/https://doi.org/10.1002/9780470027318.a5612m.
[47] S. Sahu, K. Saikia, B. Gurunathan, A. Dhakshinamoorthy, S.L. Rokhum, Green synthesis of CaO nanocatalyst using watermelon peels for biodiesel production, Mol. Catal. 547 (2023), https://doi.org/10.1016/j.mcat.2023.113342.
[48] K.N. Krishnamurthy, S.N. Sridhara, C.S. Ananda Kumar, Optimization and kinetic study of biodiesel production from Hydnocarpus wightiana oil and dairy waste scum using snail shell CaO nano catalyst, Renew. Energy 146 (2020) 280–296, https://doi.org/10.1016/j.renene.2019.06.161.
[49] M. Marquevich, S. Czernik, E. Chornet, D. Montané, Hydrogen from Biomass: Steam Reforming of Model Compounds of Fast-Pyrolysis Oil, Energy Fuels 13 (6) (1999) 1160–1166, https://doi.org/10.1021/ef990034w.
[50] B. Li, C.F. Magoua Mbeugang, Y. Huang, D. Liu, Q. Wang, S. Zhang, A review of CaO based catalysts for tar removal during biomass gasification, Energy 244 (2022), https://doi.org/10.1016/j.energy.2022.123172.
[51] R.P.B. Ramachandran, G. van Rossum, W.P.M. van Swaaij, S.R.A. Kersten, Evaporation of Biomass Fast Pyrolysis Oil: Evaluation of Char Formation, Environ. Prog. Sustain. Energy 28 (3) (2009) 410–417, https://doi.org/10.1002/ep.10388.
[52] X. Hu, G. Lu, Investigation of the steam reforming of a series of model compounds derived from bio-oil for hydrogen production, Appl. Catal., B 88(3-4) (2009) 376-385. https://doi.org/10.1016/j.apcatb.2008.10.021.